



HAL
open science

Diversity and evolution of pigment types in marine *Synechococcus* cyanobacteria

Théophile Grébert, Laurence Garczarek, Vincent Daubin, Florian Humily,
Dominique Marie, Morgane Ratin, Alban Devailly, Gregory Farrant, Isabelle
Mary, Daniella Mella-Flores, et al.

► **To cite this version:**

Théophile Grébert, Laurence Garczarek, Vincent Daubin, Florian Humily, Dominique Marie, et al..
Diversity and evolution of pigment types in marine *Synechococcus* cyanobacteria. *Genome Biology
and Evolution*, 2022, 14 (4), pp.evac035. 10.1093/gbe/evac035 . hal-03641745

HAL Id: hal-03641745

<https://hal.science/hal-03641745v1>

Submitted on 7 Oct 2022

HAL is a multi-disciplinary open access archive for the deposit and dissemination of scientific research documents, whether they are published or not. The documents may come from teaching and research institutions in France or abroad, or from public or private research centers.

L'archive ouverte pluridisciplinaire **HAL**, est destinée au dépôt et à la diffusion de documents scientifiques de niveau recherche, publiés ou non, émanant des établissements d'enseignement et de recherche français ou étrangers, des laboratoires publics ou privés.

1 **Diversity and evolution of pigment types in marine *Synechococcus***
2 **cyanobacteria**

3

4 Théophile Grébert¹, Laurence Garczarek¹, Vincent Daubin², Florian Humily¹, Dominique
5 Marie¹, Morgane Ratin¹, Alban Devailly¹, Gregory K. Farrant¹, Isabelle Mary³, Daniella Mella-
6 Flores¹, Gwenn Tanguy⁴, Karine Labadie⁵, Patrick Wincker⁶, David M. Kehoe⁷ and Frédéric
7 Partensky^{1*}

8

9 ¹Sorbonne Université, Centre National de la Recherche Scientifique, UMR 7144 Adaptation
10 and Diversity in the Marine Environment, Station Biologique, 29680 Roscoff, France;

11 ²Université Lyon 1, UMR 5558 Biometry and Evolutionary Biology, 69622 Villeurbanne,

12 France; ³Université Clermont Auvergne, CNRS, Laboratoire Microorganismes: Génome et
13 Environnement, 63000 Clermont-Ferrand, France; ⁴Centre National de la Recherche

14 Scientifique, FR 2424, Station Biologique, 29680 Roscoff, France; ⁵Genoscope, Institut de
15 biologie François-Jacob, Commissariat à l'Énergie Atomique (CEA), Université Paris-Saclay,

16 Evry, France; ⁶Génomique Métabolique, Genoscope, Institut de biologie François Jacob, CEA,
17 CNRS, Université d'Evry, Université Paris-Saclay, Evry, France; ⁷Department of Biology,

18 Indiana University, Bloomington, IN 47405, USA

19 ***Author for correspondence:** Frédéric Partensky; Sorbonne Université, Centre National de
20 la Recherche Scientifique, UMR 7144 Adaptation and Diversity in the Marine Environment,
21 Station Biologique, 29688 Roscoff, France email address: frederic.partensky@sb-roscoff.fr

22

23 Submitted to **Genome Biology and Evolution** as a research article: Revised manuscript.

24

25 **Abstract**

26 *Synechococcus* cyanobacteria are ubiquitous and abundant in the marine environment and
27 contribute for an estimated 16% of the ocean net primary productivity. Their light-harvesting
28 complexes, called phycobilisomes (PBS), are composed of a conserved allophycocyanin core
29 from which radiates six to eight rods with variable phycobiliprotein and chromophore content.
30 This variability allows *Synechococcus* cells to optimally exploit the wide variety of spectral
31 niches existing in marine ecosystems. Seven distinct pigment types or subtypes have been
32 identified so far in this taxon, based on the phycobiliprotein composition and/or the proportion
33 of the different chromophores in PBS rods. Most genes involved in their biosynthesis and
34 regulation are located in a dedicated genomic region called the PBS rod region. Here, we
35 examine the variability of gene content and organization of this genomic region in a large set
36 of sequenced isolates and natural populations of *Synechococcus* representative of all known
37 pigment types. All regions start with a tRNA-Phe_{GAA} and some possess mobile elements for
38 DNA integration and site-specific recombination, suggesting that their genomic variability relies
39 in part on a 'tycheposon'-like mechanism. Comparison of the phylogenies obtained for PBS
40 and core genes revealed that the evolutionary history of PBS rod genes differs from the core
41 genome and is characterized by the co-existence of different alleles and frequent allelic
42 exchange. We propose a scenario for the evolution of the different pigment types and highlight
43 the importance of incomplete lineage sorting in maintaining a wide diversity of pigment types
44 in different *Synechococcus* lineages despite multiple speciation events.

45

46 **Key words:** cyanobacteria, genomic island, lateral gene transfer, phycobiliprotein,
47 phycobilisome, tycheposon

48

49 **Significance**

50 The cyanobacterium *Synechococcus*, the second most abundant photosynthetic organism of
51 the ocean, has colonized all spectral niches available in this environment thanks to its
52 sophisticated and diversified light-harvesting complexes. These complexes are encoded in a
53 specialized region of the genome, the gene order and content of which are directly related to
54 the pigment type of the corresponding cells. Here, by looking at a large set of *Synechococcus*
55 genomes from strains and field populations, we highlight the extent of the genomic variability
56 of these regions within each pigment type and unveil evolutionary mechanisms that led to the
57 progressive complexification of light-harvesting antennae. Strikingly, many regions include
58 recombination and transposition genes that could have played a key role in *Synechococcus*
59 pigment diversification.

60

61 **Introduction**

62 As the second most abundant phytoplanktonic organism of the ocean, the picocyanobacterium
63 *Synechococcus* plays a crucial role in the carbon cycle, accounting for about 16% of the ocean
64 net primary productivity (Flombaum et al. 2013; Guidi et al. 2016). Members of this group are
65 found from the equator to subpolar waters and from particle-rich river mouths to optically clear
66 open ocean waters, environments displaying a wide range of nutrient concentrations,
67 temperatures, light regimes and spectral niches (Olson et al. 1990; Wood et al. 1998; Farrant
68 et al. 2016; Paulsen et al. 2016; Sohm et al. 2016; Grébert et al. 2018; Holtrop et al. 2021).
69 This ecological success is tied to the remarkably large genetic (Ahlgren and Rocap 2012;
70 Huang et al. 2012; Mazard et al. 2012; Farrant et al. 2016) and pigment diversity exhibited by
71 these cells (Six et al. 2007; Humily et al. 2013; Grébert et al. 2018; Xia et al. 2018). The pigment
72 diversity arises from wide variations in the composition of their light-harvesting antennae,
73 called phycobilisomes (PBS).

74 The building blocks of PBS are phycobiliproteins, which consist of two subunits (α and β).
75 Phycobiliproteins are assembled into trimers of heterodimers $(\alpha\beta)_3$ and then hexamers $[(\alpha\beta)_3]_2$
76 that are stacked into rod-like structures with the help of linker proteins (Yu and Glazer 1982;
77 Adir 2005). Before PBS can be assembled into their typical fan-like structure, the α and β
78 subunits must be modified by lyases that covalently attach chromophores called phycobilins,
79 at one, two or three conserved cysteine positions (Scheer and Zhao 2008; Schluchter et al.
80 2010; Bretaudeau et al. 2013). The PBS core is always made of allophycocyanin (APC), from
81 which radiate six to eight rods (Wilbanks and Glazer 1993; Sidler 1994). Three major pigment
82 types have been defined thus far based on the phycobiliprotein composition of PBS rods (Six
83 et al. 2007; Humily et al. 2013). The simplest rods are found in pigment type 1 (PT 1) and
84 contain only phycocyanin (PC), which binds the red-light absorbing phycocyanobilin (PCB,
85 $A_{\max} = 620\text{-}650$ nm; Six et al. 2007). The rods of pigment type 2 (PT 2) contain PC and
86 phycoerythrin-I (PE-I), which binds the green-light (GL) absorbing phycoerythrobilin (PEB; A_{\max}
87 = 545-560 nm). For pigment type 3 (PT 3), the rods contain the three types of phycobiliproteins,
88 PC, PE-I and phycoerythrin-II (PE-II) and bind PCB, PEB and the blue-light (BL) absorbing
89 phycourobilin (PUB, $A_{\max} = 495$ nm; Ong et al. 1984; Six et al. 2007). Although these three
90 phycobilins are isomers, PCB and PEB are created via oxidation/reduction reactions while
91 PUB is generated by the isomerization of PEB during its covalent binding to a phycobiliprotein.
92 This process is performed by dual-function enzymes called phycobilin lyase-isomerases
93 (Grébert et al. 2021).

94 Five pigment subtypes have been further defined within PT 3, depending on their
95 PUB:PEB ratio. This ratio is often approximated for living cells by the ratio of the PUB and PEB
96 fluorescence excitation peaks at 495 and 545 nm ($\text{Exc}_{495:545}$), with the emission measured at
97 585 nm. Subtype 3a strains have a fixed low $\text{Exc}_{495:545}$ ratio (< 0.6) and are often called 'GL
98 specialists', 3b strains have a fixed intermediate ratio ($0.6 \leq \text{Exc}_{495:545} < 1.6$), while 3c strains
99 display a fixed high $\text{Exc}_{495:545}$ ratio (≥ 1.6) and are often called 'BL specialists' (Six et al. 2007;
100 Sanfilippo et al. 2016). Strains belonging to subtype 3d dynamically tune their PUB:PEB ratio

101 to the ambient GL:BL ratio, a reversible physiological process known as type IV chromatic
102 acclimation (CA4; (Palenik 2001; Everroad et al. 2006; Shukla et al. 2012; Humily et al. 2013;
103 Sanfilippo et al. 2016; Sanfilippo, Garczarek, et al. 2019; Sanfilippo, Nguyen, et al. 2019). As
104 a result, the $Exc_{495:545}$ of these strains varies from 0.6 in GL to 1.6 in BL. Finally, the rare
105 subtype 3e shows only faint changes in $Exc_{495:545}$ when shifted between GL and BL (Humily et
106 al. 2013).

107 Comparative genomics analysis of the first 11 marine *Synechococcus* sequenced
108 genomes (Six et al. 2007) revealed that most genes encoding proteins involved in the
109 biosynthesis and regulation of PBS rods are grouped into a single genomic location called the
110 'PBS rod region'. These authors suggested that the gene content and organization of this
111 region was specific of the different pigment types or subtypes, but they were unable to examine
112 the degree of genomic and genetic variability for strains within each pigment type. Further
113 sequencing of additional PT 3d strain genomes revealed that CA4 capability is correlated with
114 the presence of a small genomic island that exists in one of two configurations, CA4-A and
115 CA4-B, defining the two pigment genotypes 3dA and 3dB (Humily et al. 2013). A novel
116 organization of the PBS rod region was also discovered, first from metagenomes from the
117 Baltic Sea (Larsson et al. 2014) and then from strains isolated from the Black Sea (Sánchez-
118 Baracaldo et al. 2019). Gene content analysis identified these as a new PT 2 genotype named
119 PT 2B, while the original PT 2 was renamed PT 2A. Finally, the genome sequencing of the
120 high-PUB-containing strains KORDI-100 and CC9616 showed that although they display a
121 high, PT 3c-like $Exc_{495:545}$ ratio, the gene complement, order, and alleles of their PBS rod region
122 differ from PT 3c, establishing an additional pigment subtype called PT 3f (Mahmoud et al.
123 2017; Grébert et al. 2018; Xia et al. 2018). An interesting feature of the genes within the PBS
124 rod region is that their evolutionary history apparently differs from that of the core genome (Six
125 et al. 2007; Everroad and Wood 2012; Humily et al. 2014; Grébert et al. 2018; Carrigee et al.
126 2020), but the reason(s) for this remains unclear.

127 Here, we perform a comprehensive analysis of the phylogenetic and genomic diversity of
128 *Synechococcus* pigment types by leveraging the large number of recently available genomes
129 of marine *Synechococcus* and *Cyanobium* isolates for further comparative genomic analysis.
130 We also use a targeted metagenomics approach to directly retrieve and analyze PBS rod
131 regions from natural populations as well as single-cell amplified genomes (SAGs). This
132 broadened exploration leads us to propose hypotheses for the evolution of the PBS rod regions
133 as well as for the maintenance of the wide pigment diversity found in most lineages, despite
134 multiple speciation events. This study highlights the importance of population-scale
135 mechanisms such as lateral transfers and incomplete lineage sorting in shaping the distribution
136 of pigment types among *Synechococcus* lineages.

137

138 **Results**

139 **The 5' ends of many PBS rod regions display hallmarks of 'tycheposons'** 140 **mobile genetic elements**

141 We analysed the PBS rod region from 69 *Synechococcus* and *Cyanobium* strains (Table S1),
142 which includes all PTs except 2B, which were extensively described elsewhere (Larsson et al.
143 2014; Callieri et al. 2019; Sánchez-Baracaldo et al. 2019). This dataset contains every
144 sequenced PT 3 strain and covers a very wide range of phylogenetic diversity, with
145 representatives of all three deep branches within *Cyanobacteria* Cluster 5 *sensu* Herdman et
146 al. (2001), called sub-clusters (SC) 5.1 to 5.3 (Dufresne et al. 2008; Doré et al. 2020).

147 The PBS rod region is always situated between a phenylalanine-tRNA (tRNA-Phe_{GAA}) at
148 the 5' end and the *ptpA* gene, which encodes a putative tyrosine phosphatase, at the 3' end
149 (Figure 1 and Figures S1-S7). Globally, the gene content and synteny of the PBS rod region
150 *per se* (i.e., from *unk1* to *ptpA*) is remarkably conserved among cultured representatives of a
151 given PT (Figures S1-S7). PT 1 strains have the simplest rods and the shortest PBS rod region

152 (the smallest is about 8 kb in *Cyanobium gracile* PCC 6307, Figure S1), notably containing one
153 to four copies of the *cpcBA* operon encoding α - and β -PC subunits, two to four rod linker genes
154 (one *cpcD* and up to three copies of *cpcC*; Table S2) and three phycobilin lyase genes (Table
155 S3). All other PTs possess a single *cpcBA* copy and no PC rod linker genes. In PT 2A, these
156 PC genes are replaced by a set of 16 to 18 genes necessary for the synthesis and regulation
157 of PE-I hexamers (Figure 1 and S2; Tables S2 and S3), as previously described for strain
158 WH7805 (Six et al. 2007). The main difference between the PBS rod regions of PT 2A and 3a
159 is the presence in the latter of a small cluster of five genes between *cpeR* and *cpeY*, (Figure 1
160 and Figures S2-S7). Differences between PT 3a and other PT 3 subtypes 3c, 3dA, 3dB and 3f
161 (Mahmoud et al. 2017; Xia, Guo, et al. 2017) are mainly located in the subregion between the
162 PE-II (*mpeBA*) and PE-I (*cpeBA*) operons (Figure 1). All PT 3 subtypes other than 3a possess
163 *mpeC*, encoding a PE-II associated PUB-binding linker (Six et al. 2005), inserted downstream
164 of *mpeBA*, as well as *mpeU* encoding a partially characterized phycobilin lyase-isomerase
165 (Mahmoud et al. 2017). Moreover, the conserved hypothetical gene *unk10*, which is absent
166 from all PT 3a's, is present in the middle of the PBS rod region of all 3c and 3dB PTs, while in
167 PT 3dA strains it is always located in the CA4-A island, thus outside the PBS rod region. Finally,
168 the lyase gene *mpeY* is replaced by the lyase-isomerase gene *mpeQ* in 3c and 3dB PTs
169 (Grébert et al. 2021).

170 A number of differences between PBS rod regions of various strains are more difficult to
171 link with a specific PT. This includes the putative PE-II linker gene *mpeE* present in all PT 3
172 strains except SYN20 (PT 3a) but at a highly variable position (Figure S2-S7 and Table S2).
173 Similarly, the distribution of the putative PE-II linker genes *mpeG* and *mpeH* (the latter is a
174 truncated version of the former) cannot be linked to either a PT or a clade (Table S2). It is also
175 worth noting that while all PT 3a strains contain the *rpcEF* operon, encoding the two subunits
176 of a C84 α -PC PEB lyase (Swanson et al. 1992; Zhou et al. 1992), other PT 3 subtypes may
177 have either the *rpcEF* operon or *rpcG*, a fusion gene that encodes a C84 α -PC PEB lyase-
178 isomerase and was thought to confer *Synechococcus* cells a fitness advantage in blue light

179 environments (Blot et al. 2009). This interchangeability is also found between closely related
180 strains of the same PT and clade (Figure S5-S7), and strain MINOS11 (SC 5.3/PT 3dB) even
181 possesses both genes (Figure S7). Some additional variations of ‘typical’ PBS rod regions are
182 also worth noting. Out of five PT 2A strains, only CB0205 and A15-44 possess the
183 allophycocyanin-like gene *ap1A* (Montgomery et al. 2004) which, as in all PT 3 strains, is
184 located between *unk4* and *cpcL* (Figure S2 and Table S2). CB0205 also has a unique insertion
185 of nine genes of unknown function, including *unk3*, in the middle of its PBS rod region between
186 *unk12* and *cpeF*, as observed in some natural PT 2A populations from the Baltic Sea (Larsson
187 et al. 2014).

188 A most striking and previously unreported difference between PBS regions in a number of
189 genomes is the presence of a DNA insertion of variable size between the tRNA-Phe_{GAA} and
190 *unk1* (Figure 2 and Figures S1, S3, S5-S7). In TAK9802, the 22.8 kb DNA insertion is almost
191 as large as the 24.5 kb PBS rod region. These insertions have striking similarities to
192 ‘tycheposons’, a novel type of mobile genetic elements that have been found to be responsible
193 for the translocation of 2-10 kbp fragments of heterologous DNA in *Prochlorococcus* (Hackl et
194 al. 2020). Indeed, the hallmarks of tycheposons include the systematic presence of a tRNA at
195 the 5’ end of the insertion, the localization of this insertion upstream a genomic island important
196 for niche adaptation—in the present case, adaptation to light color—and the presence in the
197 DNA insertion of a variety of mobile elements. These notably include putative tyrosine
198 recombinases, putative transposon resolvases (TnpR family) and even a complete restriction-
199 modification system (encoded by the *hsdMSR* operon; Figure 2 and Figures S1, S3, S6 and
200 S7).

201 While the genomic organization of the PBS rod region *per se*, i.e. excluding the
202 tycheposon, is broadly conserved, we found a high level of allelic diversity of the genes of this
203 region and the proteins they encode (Figures 1 and S8). The most conserved are genes
204 encoding the α - and β -subunits of phycobiliproteins. The sequence of each of these proteins
205 is at most only about 10% different from its closest ortholog. The sequences of the linker

206 proteins show greater variation between strains, with some having less than 70% identity to
207 their closest ortholog. This variability is even greater for phycobilin lyases and uncharacterized
208 conserved proteins, with some showing less than 60% sequence identity to their closest
209 orthologs (Figure S8). Such highly divergent sequences may in some cases reflect functional
210 differences, as was recently demonstrated for MpeY and MpeQ (Grébert et al. 2021) and for
211 CpeF and MpeV (Carrigee et al. 2020).

212

213 **Targeted metagenomics and SAGs reveal new PBS rod region variants and** 214 **natural deficiency mutants from field populations**

215 We investigated the genetic variability of PBS rod regions from natural *Synechococcus*
216 populations using a targeted metagenomic approach that combined flow cytometry, cell-
217 sorting, WGA and fosmid library screening (Humily et al. 2014). This method enabled us to
218 retrieve PBS rod regions from natural populations in the North Sea, northeastern Atlantic
219 Ocean and various locations within the Mediterranean Sea (Figure 3A and Table S4). In
220 addition, the high-resolution phylogenetic marker *petB* (Mazard et al. 2012) was sequenced to
221 examine the phylogenetic diversity of these natural *Synechococcus* populations. Samples
222 collected from the North Sea (fosmid libraries H1-3 in Figure 3B) and English Channel (library
223 A, previously reported by Humily et al. (2014) but re-analyzed here) were exclusively
224 composed of the cold-adapted clade I, mostly sub-clade Ib. Samples from the northeastern
225 Atlantic Ocean were co-dominated by CRD1 and either clade I (libraries G1 and G2) or the
226 environmental clades EnvA and EnvB (library E; EnvB is sometimes called CRD2; Ahlgren et
227 al. 2019). *Synechococcus* populations from the western Mediterranean Sea were largely
228 dominated by clade III (exclusively of sub-clade IIIa) at the coastal 'Point B' station located at
229 the entrance of the Bay of Villefranche-sur-Mer (<https://www.somlit.fr/villefranche/>; library F),
230 while they essentially consisted of clade I (mostly sub-clade Ib) at station A of the BOUM cruise
231 (library I2; Moutin et al. 2012) and at the long-term monitoring station BOUSSOLE located in
232 the Gulf of Lions (library I1; Antoine et al. 2008). Eastern Mediterranean Sea populations

233 collected at BOUM stations B and C were mainly from clades III, with sub-clade IIIa dominating.
234 These large differences in clade composition reflect the distinct trophic regimes of the sampled
235 sites and the diversity patterns observed here are globally consistent with previous
236 descriptions of the biogeography of *Synechococcus* clades (Zwirgmaier et al. 2008; Mella-
237 Flores et al. 2011; Paulsen et al. 2016). In particular, CRD1 and EnvB are known to co-occur
238 in iron-poor areas (Farrant et al. 2016; Sohm et al. 2016) and the northeastern Atlantic Ocean
239 has been reported to be iron-limited (Moore et al. 2013).

240 To obtain the largest possible diversity of PBS rod regions from *Synechococcus* field
241 populations, fosmid libraries generated from similar geographic areas and/or cruises and
242 showing comparable relative clade abundance profiles were pooled (as indicated in Figures
243 3A-B and Table S4) before screening and sequencing. Assembly of the eight fosmid library
244 pools resulted in the assembly of 230 contigs encompassing either a portion or all of the PBS
245 rod region. These contigs were an average size of approximately 5.5 kb and each library
246 produced at least one contig longer than 10 kb (Table S5). Each contig was assigned to a PT
247 based on its genomic organization and similarity to PBS rod regions of characterized strains
248 (Figure 1 and Figures S1-7). Most contigs corresponded to PT 3dA (145 out of 230), but all PT
249 3 subtypes represented in our reference dataset were found. There were five PT 3a contigs,
250 18 PT 3f contigs and 62 PT 3c/3dB contigs, of which nine could be unambiguously attributed
251 to PT 3c and five to PT 3dB, based on the absence or presence of a CA4-B genomic island
252 between *mpeU* and *unk10*, respectively (Figure 1).

253 A representative selection of the most complete contigs is provided in Figure 4. Most
254 contigs are syntenic with PBS rod regions from characterized strains, notably those assigned
255 to PT 3a retrieved from the North Sea (contig H3), or those assigned to PT 3f either retrieved
256 from the northeastern Atlantic Ocean (contig G16A) or from the Mediterranean Sea (all other
257 contigs assigned to PT 3f; Figure 4B). Yet, a number of contigs assigned to PT 3dA (E101,
258 F100 and F101; Figure 4A) exhibit a novel gene organization compared to reference 3dA
259 strains characterized by the insertion of a complete CA4-A genomic island between *unk3* and

260 *unk4* at the 5'-end of the PBS rod region (Figure S5). Five other contigs (G100, E28, E20, F12
261 and H104) apparently have the same organization since they possess a complete or partial
262 *mpeZ* gene located immediately upstream of *unk4*. Despite this novel location, the genes of
263 this CA4-A island are phylogenetically close to those of the PT 3dA/clade IV strains CC9902
264 or BL107 (Figure 4A). This new arrangement is found in contigs from different sequencing
265 libraries and geographically diverse samples, so it is most likely not artefactual. Contigs
266 corresponding to the canonical 3dA PBS rod region (Figure 1) were also found in most libraries
267 and contain alleles most similar to those of PT 3dA strains from either clade I or IV (Figure 4B).

268 Several contigs from the English Channel and North Sea (A1, A2, H100 and H102) that
269 displayed a similar gene organization to PT 3a strains lacked *mpeU* (Figure 4B), which
270 encodes a lyase-isomerase that attaches PUB to an as-yet undetermined residue of PEII
271 (Mahmoud et al. 2017). The absence of *mpeU* was also observed in the genome of strain
272 MVIR-18-1 (clade I/PT 3a; Figure S5A), which was shown to display a constitutively low
273 PUB:PEB ratio (Humily et al. 2013). MVIR-18-1 was isolated from the North Sea, suggesting
274 that natural populations representative of this *mpeU*-lacking variant may be common in this
275 area. Similarly, the gene organization of three contigs originating from the northeastern Atlantic
276 Ocean and assigned to CRD1 (E16A, G19A and G9B; Figure 4B) matched an unusual PBS
277 rod region found in five out of eight reference CRD1/PT 3dA strains (Figure S5A). In these
278 strains, the *mpeY* sequence is either incomplete (in MITS9508) or highly degenerate (in BIOS-
279 E4-1, MITS9504, MITS9509 and UW179A) and *fciA* and *fciB*, which encode CA4 regulators
280 (Sanfilippo et al. 2016), are missing (Figure S5B), resulting in a PT 3c phenotype (Humily et
281 al. 2013). This particular genomic organization was recently suggested to predominate in
282 CRD1 populations from warm high nutrient-low chlorophyll areas, in particular in the South
283 Pacific Ocean (Grébert et al. 2018). Thus, these contigs provide additional, more compelling
284 evidence of the occurrence of these natural variants in field populations of CRD1.

285 A number of contigs corresponding to the phylogenetically indistinguishable PBS rod
286 regions of the 3c and 3dB PTs were assembled from samples from the Mediterranean Sea

287 and the northeastern Atlantic Ocean (Figure 3B). Among these, five (C100, C40, G8D, I7 and
288 I21) could be assigned to PT 3dB due to the presence of a CA4-B genomic island between
289 *mpeU* and *unk10* (Figure 1). The gene organization of contig C100, whose alleles are most
290 similar to the PT 3dB/SC 5.3 strain MINOS11, closely resembles the unique PBS rod region
291 of this strain, which has an additional *rpcG* gene between *unk10* and *cpeZ* (Figure S7).
292 Interestingly, the CA4-B genomic island of C100 lacks *mpeW* (Figure 3B) and thus may
293 represent a novel natural variant. In contrast with the genes of contigs assigned to PT 3dA,
294 which are closely similar to clades I, IV or CRD1, those assigned to PT 3c and 3dB are most
295 closely related to representatives of different clades, including clades II, III, WPC1 and 5.3.
296 These distinct clade/PT combinations corroborate previous observations made in culture and
297 in the field (Grébert et al. 2018) and are consistent with the population composition observed
298 with *petB* at the sampling locations of these libraries (Figure 3B). Of note, some contigs from
299 fosmid library E (e.g., contig E102; PT 3c in Figure 4B) possessed alleles that were highly
300 divergent from all reference strains and likely belong to the uncultured clades EnvA or EnvB,
301 which together represented more than 30% of *Synechococcus* population in sample E (Figure
302 3B).

303 We augmented these field observations by examining the PBS rod regions contained
304 within the publicly available single-cell amplified genomes (SAGs) of marine *Synechococcus*
305 (Berube et al. 2018). Out of 50 *Synechococcus* SAGs, eleven corresponded to PT 3c, three to
306 PT 3dB, two to either PT 3c or 3dB, and 17 to PT 3dA (Figure S9 and Table S1). Using a core
307 genome phylogeny based on a set of 73 highly conserved markers (Table S6 and Figure S10),
308 we determined that these SAGs belong to clades I, II, III, IV, CRD1 as well as some rare clades,
309 including one to EnvA, one to XV, three to SC5.3, and seven to EnvB. All of the EnvB SAGs
310 contained a PBS rod region which was very similar to PT 3c except for the insertion of *rpcG*
311 between *unk10* and *cpeZ*. Due to the absence of any sequenced EnvB isolate in our reference
312 database, genes from these regions appear most similar to genes from a variety of strains and
313 clades. The same is true for SAGs from clades EnvA (AG-676-E04) and XV (AG-670-F04). All

314 SAGs assigned to PT 3dB belong to SC5.3 and possess a PBS rod region similar to that of
315 MINOS11 except for a ca. 15 kb insertion between the tRNA-Phe_{GAA} and *unk2* in AG-450-M17
316 (Figure S9B). The ten SAGs within clade CRD1 all belong to PT 3dA, but only one of these
317 contains an intact *mpeY* gene (Figure S9C). The three clade I SAGs also belong to PT 3dA.
318 Of these, AG-679-C18 provides the first example of a *mpeY* deficiency outside of clade CRD1,
319 further highlighting the prevalence of BIOS-E4-1-like populations, which are phenotypically
320 similar to (but genetically distinct from) PT 3c, in the environment (Grébert et al. 2018).
321 Interestingly, all four clade IV SAGs contain the novel PT 3dA arrangement found in several
322 fosmids, where the CA4-A genomic island is located in the PBS rod region between *unk3* and
323 *unk4*. Finally, a number of the SAGs have additional genes between the tRNA-Phe_{GAA} gene
324 and *unk1*, including recombinases, restriction enzymes, etc., sometimes in multiple copies, for
325 example in the clade II SAGs AG-670-A04 and AG-670-B23 (Figure S9A).

326 Altogether, the PBS rod regions retrieved from both fosmids and SAGs were very diverse
327 and some contained alleles whose sequences were highly diverged from those of sequenced
328 isolates. As was found in our comparative analysis of strains, the sequence diversity for lyases
329 and linker proteins was much higher than for phycobiliproteins (Figure S8).

330

331 **Genes within the PBS rod region have a very different evolutionary history than** 332 **the rest of the genome**

333 Several phylogenetic analyses based on phycobiliprotein coding genes have shown that
334 strains tend to group together according to their PT rather than their vertical (core or species)
335 phylogeny. The *cpcBA* operon enables discrimination between PT 1, 2A, 2B and 3, while the
336 *cpeBA* operon allows separation of PT 2A, 3a, 3dA, 3f and the 3c+3dB group and the *mpeBA*
337 operon is best for distinguishing between the PT 3 subtypes (Everroad and Wood 2012; Humily
338 et al. 2014; Xia, Partensky, et al. 2017; Grébert et al. 2018; Xia et al. 2018). By creating a
339 *mpeBA* phylogenetic tree using all available genomes from *Synechococcus* PT 3 strains, we

340 confirmed that alleles within a given PT 3 subtype are more closely related to one other than
341 they are to other PTs from the same clade (Figure 5, left tree). However, we also observed
342 that within each *mpeBA* clade, the tree topology actually resembles the topology based on the
343 vertically transmitted core gene *petB* (Figure 5, right tree). The few exceptions to this finding
344 could correspond to inter-clade horizontal gene transfers. The most striking example of this is
345 the clade VI strain MEDNS5, which seemingly possesses a clade III PT 3c/3dB-like *mpeBA*
346 allele (Figure 5).

347 In order to explore the evolution of the PBS genes in greater detail, we used ALE (Szöllősi
348 et al. 2013) to reconcile phylogenetic trees for each gene present in the core genome with the
349 species tree inferred from a set of 73 core genes (Table S6 and Figure S10). This comparison
350 allows the inference of evolutionary events such as duplications, horizontal transfers, losses
351 and speciations that can best explain the observed gene trees in light of the evolution of the
352 species (Figure 6). Genes from the PBS rod region experienced significantly more transfers
353 (on average 23.5 vs. 14.8 events per gene; Wilcoxon rank sum test $p=1.2 \times 10^{-13}$) and losses
354 (38.5 vs. 27.5; $p=1.7 \times 10^{-11}$) than other genes in the genome, with no significant difference in
355 gene duplications and speciations (Figure 6 and Table 1). Consistent with the observation that
356 genes within the PBS rod region are single copy except for *cpcABC* in PT 1, the increase in
357 transfers was very similar to the increase in losses. We conclude that such transfer-and-loss
358 events inferred by ALE actually correspond to allelic exchange, whereby homologous
359 recombination mediates the replacement of one allele by another.

360 Finer-grained analysis of transfer events showed that they are slightly more frequent within
361 clades for PBS genes than for other genes (9.7 vs. 8.4, $p=1.1 \times 10^{-3}$; Table 2 and Figure S11),
362 and more than twice as frequent between clades (13.9 vs. 6.1, $p=10^{-15}$; Table 2 and Figure
363 S11). As a result, most transfer events identified for PBS genes occurred between clades,
364 whereas other genes were primarily transferred within the same clade (Figure S11). We then
365 analyzed transfer events inferred for genes within the PBS rod region by their direction (Table
366 S6). The most frequent recipient of transfer (frequency of 29.07) was strain N32, which can be

367 explained by the fact that this PT 3dB strain is within a lineage of clade II that is otherwise
368 solely made up of PT 3a strains (node 177; Figure S10). The second most frequent transfer
369 recipient was strain MEDNS5 (clade VI; frequency=23.71), which possesses the allele of a PT
370 3c/3dB strain of clade III, as exemplified with *mpeBA* (Figure 5). Strains RS9902 and A15-44,
371 both within clade II, were the third (21.69) and fourth (18.79) most frequent recipient strains.
372 A15-44 belongs to PT 2, a quite rare PT among strictly marine SC 5.1 *Synechococcus* strains
373 (Grébert et al. 2018), and indeed groups in the tree with the PT 3c strain RS9902 (Figure S10).
374 The apparent high transfer frequency to RS9902 could thus represent transfers of PT 2 to the
375 ancestor of RS9902 and A15-44 (node 103 in Figure S10 and Table S7), followed by transfer
376 of PT 3c to RS9902. Other strains for which high frequency of transfers were inferred are
377 KORDI-49 (WPC1/3aA), RCC307 (SC 5.3/3eA), WH7803 (V/3a), CB0205 (SC 5.2/2), which
378 all represent rare combinations of clade and PT (Figure S10 and Table S7). Internal nodes
379 with high frequency of transfers were mostly deep-branching, representing the ancestor of SC
380 5.3, clades I, V, VI, VII and CRD1, 5.1B, and 5.1A (nodes 171, 189, 191, 197, with frequencies
381 of 22.2, 14.5, 13.9 and 12.9, respectively). Taken together, these results indicate that genes
382 of the PBS rod region have a very ancient evolutionary history marked by frequent
383 recombination events both within and between *Synechococcus* clades.

384

385 Discussion

386 The variable gene content of the PBS rod region might partly rely on a tycheposon-like 387 mechanism

388 Most of the current knowledge about the genomic organization and genetic diversity of the
389 *Synechococcus* PBS rod region has relied on analysis of the first 11 sequenced genomes (Six
390 et al. 2007) and later analyses of metagenomic assemblages or strains retrieved from a few
391 specific locations. These include the SOMLIT-Astan station in the English Channel (Humily et
392 al. 2014), the Baltic and Black Seas, where a new organization of the PBS rod region (PT 2B)
393 was found associated with SC 5.2 populations (Larsson et al. 2014; Callieri et al. 2019), and
394 freshwater reservoirs dominated by PT 2A/SC 5.3 populations (Cabello-Yeves et al. 2017).
395 Here, we analyzed a wide set of *Synechococcus* and *Cyanobium* genomes (69 genomes and
396 33 SAGs; Table S1) as well as PBS rod regions directly retrieved from a variety of trophic and
397 light environments (229 contigs; Table S4). Together, these cover all of the genetic and PT
398 diversity currently known for this group (except PT 2B), enabling us to much better assess the
399 extent of the diversity within each PBS rod region type.

400 While our data confirmed that the gene content and organization of this region are highly
401 conserved within a given PT, independent of its phylogenetic position (Six et al. 2007), they
402 also highlighted some significant variability within each PT. We notably unveiled a novel and
403 evolutionary important trait of PBS rod regions, namely the frequent presence of DNA
404 insertions between the tRNA-Phe_{GAA} and *unk1* in both strains or SAGs (Figure 2 and Figures
405 S1-S7 and S9). These insertions share striking similarities to ‘tycheposons’, a novel type of
406 mobile genetic elements recently discovered in *Prochlorococcus* (Hackl et al. 2020). This
407 notably includes the hallmark presence of a tRNA and, in many of them, of the complete or
408 partial tyrosine recombinase gene. However, *Prochlorococcus* tycheposons have been
409 associated with seven possible tRNA types (Hackl et al. 2020), but never with a tRNA-Phe_{GAA},
410 which is the tRNA type systematically found upstream of PBS rod regions. Also, while in

411 *Prochlorococcus* the tyrosine recombinase is most often located immediately downstream the
412 tRNA at the 5' end of the tycheposon, in *Synechococcus* it is found at the distal end of the
413 tycheposon. Closer examination of this distal region in several *Synechococcus* genomes
414 (notably in TAK9802) revealed a remnant of tRNA-Phe_{GAA} located between the tyrosine
415 recombinase gene and *unk1* in genomes where the former gene was complete. This
416 observation strongly suggests that insertion of DNA material occurred by homologous
417 recombination via a site-specific integrase at the level of this tRNA, since this process often
418 leaves the integrated elements flanked on both sides with the attachment site motif (Grindley
419 et al. 2006). The presence of other recombinases in the DNA insertion in a few *Synechococcus*
420 strains, such as putative site-specific, gamma-delta resolvases (*tnpR*-like genes in Figures 2
421 and S1, S3A, S6 and S7) may have resulted from iterative integrations at the same tRNA site,
422 a phenomenon also reported for *Prochlorococcus* tycheposons (Hackl et al. 2020). We
423 hypothesize that some of the specific genes present in PBS rod regions, notably the thirteen
424 unknown genes (*unk1-13*; Fig. 1 and Figures S1-S7), could have been acquired by lateral
425 transfer into this specific tycheposon then transposition into the PBS rod region. These genes
426 could have been retained by natural selection because of their yet unknown role in PBS
427 biosynthesis or regulation. Additionally, by facilitating the import of foreign DNA as flanking
428 material to mobile genetic elements (Hackl et al. 2020), tycheposons could also have played
429 a key role in the conservation of the wide genomic diversity of PBS rod regions, and thus
430 pigment type diversity, despite the multiple speciation events that occurred in the
431 *Synechococcus* lineage, generating the three sub-clusters and many clades observed
432 nowadays in this radiation.

433

434 **Novel insights into the evolution of CA4 islands and chromatic acclimation**

435 The characterization of many PBS rod regions from the environment that were retrieved from
436 SAGs or fosmids led us to the discovery of a new location for the CA4-A genomic island near

437 the 5'-end of the PBS rod region (Figure 4A and S9C) rather than elsewhere, as found in the
438 genomes of all 3dA strains sequenced thus far (Figure S5B). All of the genes of the PBS rod
439 region containing these atypical CA4-A islands have strongest similarity to the corresponding
440 genes in canonical PT 3dA strains. Therefore, this new organization is unlikely to correspond
441 to a new PT phenotype/genotype but rather to a previously unidentified PT 3dA variant. The
442 localization of the CA4-A region at the 5'-end of the PBS rod region strongly supports the
443 abovementioned hypothesis that the increases in the complexity of *Synechococcus*
444 pigmentation by progressive extension of the PBS rod region primarily occurred via a
445 tychepon mechanism. This finding also provides a simple solution to the paradox of how two
446 physically separate genomic regions encoding related and interacting components, with
447 evolutionary histories that differ from the rest of the genome, were still able to co-evolve.

448 The CA4-A island not only has a highly variable position within the genome, but its gene
449 content is also variable. Indeed, five out of eight CRD1 strains with a 3dA configuration of the
450 PBS rod region possess an incomplete CA4-A island (Figure S5B). In contrast, the CA4-B
451 island is always found at the same position in the genome and is complete in all 3dB strains
452 sequenced so far (Figure S7). If the CA4-B island also has been generated in a tychepon,
453 the mechanism by which it has been transposed in the middle of the PBS rod region remains
454 unknown, since there are no known recombination hotspots in this region. Contig C100, which
455 appears to lack the PEB lyase-encoding gene *mpeW* (Figure 4B; Grébert et al. 2021), is the
456 first documented example of an incomplete CA4-B region. We predict that this new genotype
457 has a constitutively high PUB:PEB ratio since this organism is likely to contain an active lyase-
458 isomerase MpeQ (Grébert et al. 2021). It also has a *rpcG* gene encoding a PC lyase-isomerase
459 (Blot et al. 2009) located immediately downstream of the CA4-B island and on the same strand
460 as *unk10* (Figures 4B and S7). This arrangement, which has thus far only been observed in
461 MINOS11, suggests that *rpcG* expression could be controlled by light color and its protein
462 product compete with those encoded by the *rpcE-F* operon, since both act on the same
463 cysteine residue of α -PC (Swanson et al. 1992; Zhou et al. 1992; Blot et al. 2009). This

464 arrangement would be similar to the relationship between *mpeZ* and *mpeY* (Sanfilippo,
465 Nguyen, et al. 2019) or between *mpeW* and *mpeQ* (Grébert et al. 2021). If confirmed, this
466 would be the first case of chromatic acclimation altering the chromophorylation of PC instead
467 of PE-I and PE-II in marine *Synechococcus*.

468

469 **A hypothesis for the evolution of the PT 3 PBS rod region**

470 The apparent mismatch between PBS pigmentation and vertical phylogeny raises the
471 intriguing question of how different PTs have evolved and been maintained independently from
472 the extensive clade diversification. It is generally agreed that the occurrence of the *mpeBA*
473 operon in marine *Synechococcus* spp. PT 3 and the closely related uncultured *S. spongiarum*
474 group resulted from gene duplication and divergence of a pre-existing *cpeBA* operon (Apt et
475 al. 1995; Everroad and Wood 2012; Sánchez-Baracaldo et al. 2019). Yet phycobiliproteins are
476 part of a complex supramolecular structure, interacting with many other proteins such as
477 linkers, phycobilin lyases and regulators, which all need to co-evolve. Here, we propose an
478 evolutionary scenario of progressively increasing complexity for the diversification of PT 3 from
479 a PT 2/3 precursor (Figure 7). Our model integrates recent advances in our understanding of
480 the functional characterization of PBS gene products, notably phycobilin lyases (Shukla et al.
481 2012; Sanfilippo et al. 2016; Mahmoud et al. 2017; Kronfel et al. 2019; Sanfilippo, Nguyen, et
482 al. 2019; Carrigee et al. 2020; Grébert et al. 2021). Our proposal does not include PT 2B since
483 strains exhibiting this PT generally possess several phycocyanin operons, such as PT 1
484 (Callieri et al. 2019), and it cannot be established with certainty whether of PT 2B or PT 2A
485 occurred first.

486 The first step toward PE-II acquisition by the PT 2/3-like precursor involved the generation
487 of a *mpeBA* operon precursor by duplication and divergence from an ancestral *cpeBA* operon.
488 This was accompanied by the concomitant duplication of the ancestral the PE-I specific lyase
489 gene *cpeY* and its divergence to a precursor of the PEII-specific *mpeY* lyase gene (Figure 7).

490 The origin of the *unk8/7* fusion gene and *unk9*, occurring at the 5'-end of the PE-II subregion
491 in all PT 3 strains (Figure 1 and Figure S2), is more difficult to assess. However, it is noteworthy
492 that Unk9 and the two moieties of Unk8/7 all belong to the Nif11-related peptide (N11P) family,
493 which shows extensive paralogous expansion in a variety of cyanobacteria (Haft et al. 2010).
494 Although some members of the N11P family have been suggested to be secondary metabolite
495 precursors (Haft et al. 2010; Tang and van der Donk 2012; Cubillos-Ruiz et al. 2017), the
496 functions of the Unk8/7 and Unk9 peptides remains unclear. Yet the localization of their genes
497 in the PE-II sub-region of all PT 3 strains strongly suggests a critical role in PE-II biosynthesis
498 or regulation. One possibility is that they modulate the specificity of some PE-I lyases to extend
499 their activity to PE-II subunits. Another, more subtle, change that occurred during the evolution
500 of PT 3 was the change in the N-terminal part of the MpeD linker to include a specific insertion
501 of 17 amino acids near the N-terminal region that is involved in PUB binding, as found in all
502 PEII-specific linkers (Six et al. 2005). Present-day PT 3a would have directly descended from
503 this PT 2/3 last common ancestor (LCA). Accordingly, the PBS rod region from PT 3a is the
504 simplest of all PT 3 and PT 3a sequences form the most basal clade in both *mpeBA* and
505 *mpeWQYZ* phylogenies when these are rooted using *cpeBA* and *cpeY* sequences respectively
506 (Figure 3C).

507 The three main differences between the PT 2/3 LCA and other PT 3 LCAs are the
508 acquisition of the linker gene *mpeC*, which most likely resulted from the duplication and
509 divergence of a pre-existing PE-I linker (either *cpeC* or *cpeE*), the acquisition of *unk10*,
510 encoding an additional member of the N11P family, and the replacement of *cpeF* by *mpeU*
511 (Figure 7). The lyase-isomerase MpeU belongs to the same family as the PEB lyase CpeF and
512 is likely to have been derived from it. Even though the CpeF/MpeU phylogeny is unclear due
513 to the deep tree branches having low bootstrap supports (Mahmoud et al. 2017; Carrigee et
514 al. 2020), we hypothesize that the PT 3f/c/dB/dA precursor already had a *mpeU*-like gene.
515 Phylogenetic trees of *mpeBA* and of the *mpeWQYZ* enzyme family places the recently
516 described PT 3f (Xia et al. 2018) in a branch between those formed by PT 3a in one case and

517 PT 3dA and 3c/3dB sequences in the other (Figure 3C). Consistently, the organization of the
518 PT 3f PBS rod region appears to be intermediate between PT 3a and the more complex PT
519 3c/3dB/3dA regions. The only difference between the PT 3f/c/dB/dA precursor and the present-
520 day PT 3f would be the loss of *unk11*, a short and highly variable open reading frame (Figure
521 7).

522 The PT 3f/c/dB/dA LCA then would have evolved to give the common precursor of PT
523 3dA/c/dB. This step likely involved four events: i) the splitting of the *unk8/7* gene into two
524 distinct genes, *unk8* and *unk7*, ii) the duplication of *mpeU* followed by iii) a tandem
525 translocation of one *mpeU* gene copy and *cpeZ* between *mpeC* and *cpeY*, and iv) the
526 divergence of the second *mpeU* copy to give *mpeV*, encoding another recently characterized
527 lyase-isomerase of the CpeF family (Carrigee et al. 2020). Again, the poor bootstrap support
528 of deep branches of the CpeF/MpeU/MpeV phylogeny (Carrigee et al. 2020) makes it difficult
529 to confirm this hypothesis, and we cannot exclude the possibility that *mpeV* was derived
530 directly from *cpeF*. Since the 3dA-type PBS rod region does not exist in present-day
531 *Synechococcus* spp. without co-occurrence of a CA4-A island, the proto-CA4 island must also
532 have evolved concurrently with the PT 3dA precursor. The two regulatory genes it contains,
533 *fciA* and *fciB*, likely originate from the duplication and divergence of an ancestral *fci* precursor
534 gene encoding a member of the AraC family. Both FciA and FciB possess a AraC-type C-
535 terminal helix-turn-helix domain, yet their N-terminal domains have no similarity to any known
536 protein (Humily et al. 2013; Sanfilippo et al. 2016). Generation of a complete CA4-A genomic
537 island required three steps: i) a translocation of *unk10* into the proto-CA4 genomic island, ii)
538 acquisition of *fciC*, a putative ribbon helix-helix domain-containing regulator that has similarity
539 to bacterial and phage repressors (Humily et al. 2013), and iii) acquisition of *mpeZ*, possibly
540 by duplication and divergence of *mpeY*, then translocation into the proto-CA4-A genomic island
541 (Figure 7). It would also require the acquisition of the proper regulatory elements that are still
542 unidentified.

543 Creation of the PT 3c-type PBS rod region from the same precursor that led to PT 3dA
544 required three events: i) the loss of *mpeV*, ii) the translocation of *unk10* between *mpeU* and
545 *cpeZ*, and iii) the divergence of the pre-existing lyase gene *mpeY* to make the lyase-isomerase
546 gene *mpeQ* (Grébert et al. 2021). Then, the development of the PT 3dB from a PT 3c precursor
547 only required the incorporation of a CA4-B genomic island in which the *mpeW* gene likely
548 originated, like *mpeZ*, from duplication and divergence of *mpeY*, then translocation into the
549 genomic island.

550 As previously noted, PTs 3c and 3dB share the same alleles for all PBS genes. Their
551 only difference is the insertion of the CA4-B genomic island within the PBS rod region. Thus,
552 conversion between these two PTs appears to be relatively straightforward and may occur
553 frequently. In contrast, the PT 3a and 3dA PBS-encoding regions differ by a number of genes
554 and often have different alleles for orthologous genes. Thus, although the acquisition of a CA4-
555 A island theoretically should be sufficient to transform a PT 3a-type green light specialist into
556 a chromatic acclimater (Sanfilippo, Garczarek, et al. 2019; Sanfilippo, Nguyen, et al. 2019;
557 Grébert et al. 2021), the divergence between the PT 3a and 3dA PBS components could make
558 this conversion problematic. In accordance with this, although a number of PT 3a strains have
559 naturally acquired either a complete (MVIR-18-1) or a partial (WH8016 and KORDI-49) CA4-
560 A genomic island (so-called PT 3aA strains), none exhibit a functional CA4 phenotype (Choi
561 and Noh 2009; Humily et al. 2013).

562

563 **Incomplete Lineage Sorting explains PBS genes phylogeny**

564 The inconsistency between phylogenies obtained from PBS and core genes has led several
565 authors to suggest that frequent lateral gene transfer (LGT) events of parts of or the whole
566 PBS rod region likely occurred during the evolution of *Synechococcus* (Six et al. 2007;
567 Dufresne et al. 2008; Haverkamp et al. 2008; Everroad and Wood 2012; Sánchez-Baracaldo
568 et al. 2019). However, by examining additional representatives of each PT/clade combination

569 in this manuscript, we have shown that different alleles of the PBS genes correspond to the
570 different PTs, and that the evolutionary history of each of these alleles is finely structured and
571 globally consistent with the core phylogeny (Figure 5). This suggests that LGT events between
572 clades are actually rare. An unambiguous LGT event occurred in strain MEDNS5 (PT 3c, clade
573 VIa), since its *mpeBA* sequence clustered with PT 3c/clade III *mpeBA* sequences (Figure 5
574 and Table S7). Similar observations were made for other PBS genes such as *cpeBA*,
575 *mpeW/Y/Z* and *mpeU* (Humily et al. 2013; Mahmoud et al. 2017; Grébert et al. 2018). This
576 suggests that there have been transfers of blocks of co-functioning genes. The match between
577 the evolutionary history of each allele and the corresponding core phylogeny also suggests
578 that most transfer events occurred very early during the diversification of marine
579 *Synechococcus*. Indeed, the reconciliation analysis using ALE detected a high frequency of
580 transfers to very ancient lineages in *Synechococcus* phylogeny (Figure S10 and Table S7).
581 However, the reconciliation model implemented in ALE does not account for incongruences
582 between gene trees and species trees arising when an ancestral polymorphism in a population
583—in the present case, occurrence of several alleles—is not fully sorted (i.e., resolved into
584 monophyletic lineages) after a speciation event. This is because of the stochastic way in which
585 lineages inherit alleles during speciation (Tajima 1983; Galtier and Daubin 2008; Lassalle et
586 al. 2015), and such incongruences are interpreted by ALE as replacement transfers (i.e., a
587 transfer and a loss). This phenomenon, called ‘incomplete lineage sorting’ (ILS), is predicted
588 to occur for at least some genes in a genome and is expected to be particularly important in
589 prokaryotes with large population sizes (Retchless and Lawrence 2007; Degnan and
590 Rosenberg 2009; Retchless and Lawrence 2010). In fact, the coalescent time (i.e. time to the
591 last common ancestor), and hence the frequency of ILS, is predicted to be proportional to the
592 effective population size (Abby and Daubin 2007; Batut et al. 2014). Since *Synechococcus* is
593 the second most abundant photosynthetic organism in the oceans (Flombaum et al. 2013), we
594 can reasonably expect to observe some ILS in this lineage. Assuming that the *Synechococcus*
595 effective population size is the same order of magnitude as that estimated for *Prochlorococcus*
596 (10^{11} cells; Baumdicker et al. 2012; Batut et al. 2014; Kashtan et al. 2014) and that

597 *Synechococcus* has a generation time of about one day, a tentative allelic fixation time would
598 be of about 280 million years (My). This rough estimate is on the same order of timescale as
599 the divergence between SC 5.3 and SC 5.2/SC 5.1 (400-880 My ago) or, within SC 5.1,
600 between marine *Synechococcus* and *Prochlorococcus* (270-620 My ago; Sánchez-Baracaldo
601 et al. 2019). This further supports the possibility of ILS being the major source of the apparent
602 incongruence in PT distribution between clades (Retchless and Lawrence 2007). This new
603 evolutionary scenario would imply that the different PTs appeared before the diversification of
604 SC 5.1 clades, and very likely before the divergence of SC 5.1 and 5.3, as was also recently
605 suggested (Sánchez-Baracaldo et al. 2019). The basal position of the two SC 5.3 isolates in
606 the phylogeny of the different *mpeBA* alleles (Figure 5) and the recent discovery of *mpeBA*-
607 possessing *Prochlorococcus* (Ulloa et al. 2021) reinforce this hypothesis. In this view,
608 *Synechococcus* clades were derived from an ancestral population in which all PT 3 (a through
609 f) co-existed. Some clades seem to have lost some PTs in the course of their separation from
610 other clades such as clade IV or CRD1, in which we only observe isolates of PT 3dA. Others
611 might have conserved most pigment types, such as clade II, which encompasses all PT 3
612 except 3dA. Thus, recombination would maintain intra-clade diversity (Lassalle et al. 2015),
613 while allowing clades to expand to novel niches defined by environmental parameters such as
614 iron availability or phosphate concentration (Doré et al. 2020). This would have allowed the
615 partial decoupling of adaptation to multiple environmental factors from adaptation to light color
616 (Retchless and Lawrence 2007; Retchless and Lawrence 2010). In this regard, the occurrence
617 of tycheposon-like elements at the 5' end of many PBS rod regions is particularly interesting
618 as it could provide *Synechococcus* populations with a tool favouring intra-clade recombination.

619 In conclusion, the analyses of the PBS rod region of newly sequenced *Synechococcus*
620 isolates and of those retrieved from wild populations allowed us to clarify previous findings
621 regarding the relationships between gene content and organization of this region, allelic
622 variability and *Synechococcus* PTs. We proposed a scenario for the evolution of the different
623 PTs and present a new hypothesis based on population genetics to explain the observed

624 discrepancies between PT and core phylogenies. These results demonstrate that analyzing
625 *Synechococcus* evolution from the perspective of its demographic history provides a promising
626 avenue for future studies.

627

628 **Materials and methods**

629 **Genome information**

630 Genomic regions used in this study were obtained from 69 public complete or draft genomes
631 (Dufresne et al. 2008; Cubillos-Ruiz et al. 2017; Lee et al. 2019; Doré et al. 2020). Information
632 about these genomes can be found in Table S1.

633 **Fosmid libraries**

634 Samples for construction of the fosmid library were collected during oceanographic cruises
635 CEFAS (North Sea), BOUM (Mediterranean Sea) and the RRS Discovery cruise 368
636 (northeastern Atlantic Ocean) as well as from three long-term observatory sites. Two belong
637 to the “Service d'Observation en Milieu Littoral” (SOMLIT), Astan located 2.8 miles off Roscoff
638 and ‘Point B’ at the entrance of the Villefranche-sur-mer Bay, while the ‘Boussole’ station is
639 located 32 miles off Nice in the Ligurian current (Antoine et al. 2008). Details on the sampling
640 conditions, dates and locations are provided in Table S4. Pyrosequencing of the *petB* gene,
641 cell sorting, DNA extraction, whole genome amplification, fosmid library construction,
642 screening and sequencing were performed as previously described (Humily et al. 2014) and
643 the fosmid libraries previously obtained from the Astan station were re-assembled using a
644 different approach, as described below.

645 Sequencing reads were processed using BioPython v.1.65 (Cock et al. 2009) to trim bases
646 with a quality score below 20, after which reads shorter than 240 nt or with a mean quality
647 score below 27 were discarded. Reads corresponding to the fosmid vector, the *E. coli* host or
648 contaminants were removed using a BioPython implementation of NCBI VecScreen

649 (<https://www.ncbi.nlm.nih.gov/tools/vecscreen/about/>). Paired-reads were merged using
650 FLASH v1.2.11 (Magoč and Salzberg 2011), and merged and non-merged remaining reads
651 were assembled using the CLC AssemblyCell software (CLCBio, Prismet, Denmark).
652 Resulting contigs were scaffolded using SSPACE v3.0 (Boetzer et al. 2011), and scaffolds
653 shorter than 500 bp or with a sequencing coverage below 100x were removed. To reduce the
654 number of contigs while preserving the genetic diversity, a second round of scaffolding was
655 done using Geneious v6.1.8 (Biomatters, Auckland, New Zealand). Assembly statistics are
656 reported in Table S5. Assembled scaffolds were manually examined to control for obvious
657 WGA-induced as well as assembly chimeras. Annotation of PBS genes was performed
658 manually using Geneious and the Cyanorak v2.0 information system ([http://www.sb-](http://www.sb-roscoff.fr/cyanorak/)
659 [roscoff.fr/cyanorak/](http://www.sb-roscoff.fr/cyanorak/)). Plotting of regions was conducted using BioPython (Cock et al. 2009).

660 **Phylogenetic analyses**

661 Sequences were aligned using MAFFT v7.299b with the G-INS-i algorithm (default
662 parameters; (Kato and Standley 2013). ML phylogenies were reconstructed using PhyML
663 v20120412 using both SPR and NNI moves (Guindon and Gascuel 2003). Phylogenetic trees
664 were plotted using Python and the ETE Toolkit (Huerta-Cepas et al. 2016).

665 **Inference of evolutionary events**

666 Species (vertical) phylogeny was inferred from a set of 73 conserved marker genes (Table S6;
667 (Wu et al. 2013). For each marker gene, protein sequences were extracted from 69 isolate
668 genomes and 33 *Synechococcus* SAGs (Table S1; Berube et al. 2018), aligned using MAFFT,
669 and the alignment trimmed using trimAl (Capella-Gutiérrez et al. 2009). Alignments were
670 concatenated into a multiple alignment which was used for reconstruction of the species tree.
671 Phylogenetic reconstruction was done using RAxML 8.2.9, with 100 searches starting from
672 randomized maximum parsimony trees and 100 searches from fully random trees (Stamatakis
673 2014). Best tree was selected and 200 bootstraps computed. Next, gene trees were inferred
674 for every gene present in more than half of the considered genomes. For each gene, protein
675 sequences were extracted from genomes and aligned using MAFFT. The resulting alignment

676 was used for phylogenetic reconstruction with RAxML, and 100 bootstraps computed.
677 Evolutionary events (gene duplication, transfer, loss or speciation) were inferred for each gene
678 from these bootstraps using ALE v0.4, which uses a maximum-likelihood framework to
679 reconcile gene trees with the species tree (Szöllősi et al. 2013).

680

681 **Acknowledgments**

682 This work was supported by the collaborative program METASYN with the Genoscope, the
683 French “Agence Nationale de la Recherche” programs CINNAMON (ANR-17-CE02-0014-01)
684 and EFFICACY (ANR-19-CE02-0019) as well as the European Union program Assemble+
685 (Horizon 2020, under grant agreement number 287589) to F.P and L.G. and by National
686 Science Foundation Grants (U.S.A.) MCB-1029414 and MCB-1818187 to D.M.K. We thank
687 Fabienne Rigaud-Jalabert for collecting sea water, Thierry Cariou for providing physico-
688 chemical parameters from the SOMLIT-Astan station and Thomas Hackl for useful discussions
689 about tycheposons. We are also most grateful to the Biogenouest genomics core facility in
690 Rennes (France) for *petB* sequencing and the platform of the Centre National de Ressources
691 Génomiques Végétales in Toulouse (France) for fosmid library screening. We also warmly
692 thank the Roscoff Culture Collection for maintaining and isolating some of the *Synechococcus*
693 strains used in this study as well as the ABIMS Platform (Station Biologique de Roscoff) for
694 help in setting up the genome database used in this study and for providing storage and
695 calculation facilities for bioinformatics analyses.

696

697 **Data Availability:** The genomic data underlying this article are available in Genbank and
698 accession numbers are provided in Table S1. Annotated fosmid sequence data are available
699 online at https://figshare.com/collections/Diversity_and_evolution_of_light-

700 [harvesting complexes in marine *Synechococcus cyanobacteria*/5607200](#). Other data are
701 available in the article and in its online supplementary material.

702

703 **References**

- 704 Abby S, Daubin V. 2007. Comparative genomics and the evolution of prokaryotes. *Trends Microbiol*
705 15:135–141.
- 706 Adir N. 2005. Elucidation of the molecular structures of components of the phycobilisome:
707 Reconstructing a giant. *Photosynth Res* 85:15–32.
- 708 Ahlgren NA, Belisle BS, Lee MD. 2019. Genomic mosaicism underlies the adaptation of marine
709 *Synechococcus* ecotypes to distinct oceanic iron niches. *Environ Microbiol* 22:1801–1815.
- 710 Ahlgren NA, Rocap G. 2012. Diversity and distribution of marine *Synechococcus*: Multiple gene
711 phylogenies for consensus classification and development of qPCR assays for sensitive
712 measurement of clades in the ocean. *Front Microbiol* 3:213–213.
- 713 Antoine D, d’Ortenzio F, Hooker SB, Bécu G, Gentili B, Tailliez D, Scott AJ. 2008. Assessment of
714 uncertainty in the ocean reflectance determined by three satellite ocean color sensors (MERIS,
715 SeaWiFS and MODIS-A) at an offshore site in the Mediterranean Sea (BOUSSOLE project). *J Geophys*
716 *Res* 113:C07013.
- 717 Apt KE, Collier JL, Grossman AR. 1995. Evolution of the phycobiliproteins. *J Mol Biol* 248:79–96.
- 718 Batut B, Knibbe C, Marais G, Daubin V. 2014. Reductive genome evolution at both ends of the bacterial
719 population size spectrum. *Nat Rev Microbiol* 12:841–850.
- 720 Baumdicker F, Hess WR, Pfaffelhuber P. 2012. The infinitely many genes model for the distributed
721 genome of bacteria. *Genome Biol. Evol.* 4:443–456.
- 722 Berube PM, Biller SJ, Hackl T, Hogle SL, Satinsky BM, Becker JW, Braakman R, Collins SB, Kelly L, Berta-
723 Thompson J, et al. 2018. Single cell genomes of *Prochlorococcus*, *Synechococcus*, and sympatric
724 microbes from diverse marine environments. *Sci Data* 5:180154.
- 725 Blot N, Wu X-J, Thomas J-C, Zhang J, Garczarek L, Böhm S, Tu J-M, Zhou M, Plöscher M, Eichacker L, et
726 al. 2009. Phycourobilin in trichromatic phycocyanin from oceanic cyanobacteria is formed post-
727 translationally by a phycoerythrobilin lyase-isomerase. *J Biol Chem* 284:9290–9298.
- 728 Boetzer M, Henkel CV, Jansen HJ, Butler D, Pirovano W. 2011. Scaffolding pre-assembled contigs using
729 SSPACE. *Bioinformatics* 27:578–579.

- 730 Bretaudeau A, Coste F, Humily F, Garczarek L, Le Corguillé G, Six C, Ratin M, Collin O, Schluchter WM,
731 Partensky F. 2013. Cyanolyase: a database of phycobilin lyase sequences, motifs and functions.
732 *Nucl Acids Res* 41:D396–D401.
- 733 Cabello-Yeves PJ, Haro-Moreno JM, Martin-Cuadrado AB, Ghai R, Picazo A, Camacho A, Rodriguez-
734 Valera F. 2017. Novel *Synechococcus* genomes reconstructed from freshwater reservoirs. *Front*
735 *Microbiol* 8:1151.
- 736 Callieri C, Slabakova V, Dzhembekova N, Slabakova N, Peneva E, Cabello-Yeves PJ, Di Cesare A, Eckert
737 EM, Bertoni R, Corno G, et al. 2019. The mesopelagic anoxic Black Sea as an unexpected habitat for
738 *Synechococcus* challenges our understanding of global “deep red fluorescence.” *ISME J* 13:1676–
739 1687.
- 740 Capella-Gutiérrez S, Silla-Martínez JM, Gabaldón T. 2009. trimAl: a tool for automated alignment
741 trimming in large-scale phylogenetic analyses. *Bioinformatics* 25:1972–1973.
- 742 Carrigee LA, Frick JP, Karty JA, Garczarek L, Partensky F, Schluchter WM. 2020. MpeV is a lyase
743 isomerase that ligates a doubly-linked phycourobilin on the β -subunit of phycoerythrin I and II in
744 marine *Synechococcus*. *J Biol Chem* 296:100031.
- 745 Choi DH, Noh JH. 2009. Phylogenetic diversity of *Synechococcus* strains isolated from the East China
746 Sea and the East Sea. *FEMS Microbiol Ecol* 69:439–448.
- 747 Cock PJA, Antao T, Chang JT, Chapman BA, Cox CJ, Dalke A, Friedberg I, Hamelryck T, Kauff F, Wilczynski
748 B, et al. 2009. Biopython: Freely available Python tools for computational molecular biology and
749 bioinformatics. *Bioinformatics* 25:1422–1423.
- 750 Cubillos-Ruiz A, Berta-Thompson JW, Becker JW, van der Donk WA, Chisholm SW. 2017. Evolutionary
751 radiation of lanthipeptides in marine cyanobacteria. *Proc Natl Acad Sci USA* 114:E5424–E5433.
- 752 Degnan JH, Rosenberg NA. 2009. Gene tree discordance, phylogenetic inference and the multispecies
753 coalescent. *Trends Ecol Evol* 24:332–340.
- 754 Doré H, Farrant GK, Guyet U, Haguait J, Humily F, Ratin M, Pitt FD, Ostrowski M, Six C, Brillet-Guéguen
755 L, et al. 2020. Evolutionary mechanisms of long-term genome diversification associated with niche
756 partitioning in marine picocyanobacteria. *Front Microbiol* 11:567431.
- 757 Dufresne A, Ostrowski M, Scanlan DJ, Garczarek L, Mazard S, Palenik BP, Paulsen IT, de Marsac NT,
758 Wincker P, Dossat C, et al. 2008. Unraveling the genomic mosaic of a ubiquitous genus of marine
759 cyanobacteria. *Genome Biol* 9:R90.
- 760 Everroad C, Six C, Partensky F, Thomas J-C, Holtzendorff J, Wood AM. 2006. Biochemical bases of Type
761 IV chromatic adaptation in marine *Synechococcus* spp. *J Bacteriol* 188:3345–3356.
- 762 Everroad RC, Wood AM. 2012. Phycoerythrin evolution and diversification of spectral phenotype in
763 marine *Synechococcus* and related picocyanobacteria. *Mol Phylogen Evol* 64:381–392.

- 764 Farrant GK, Doré H, Cornejo-Castillo FM, Partensky F, Ratin M, Ostrowski M, Pitt FD, Wincker P, Scanlan
765 DJ, Ludicone D, et al. 2016. Delineating ecologically significant taxonomic units from global patterns
766 of marine picocyanobacteria. *Proc Natl Acad Sci USA* 113:E3365–E3374.
- 767 Flombaum P, Gallegos JL, Gordillo R a, Rincón J, Zabala LL, Jiao N, Karl DM, Li WKW, Lomas MW,
768 Veneziano D, et al. 2013. Present and future global distributions of the marine Cyanobacteria
769 *Prochlorococcus* and *Synechococcus*. *Proc Natl Acad Sci USA* 110:9824–9829.
- 770 Galtier N, Daubin V. 2008. Dealing with incongruence in phylogenomic analyses. *Phil Trans Roy Soc B*
771 *Biol Sci* 363:4023–4029.
- 772 Grébert T, Doré H, Partensky F, Farrant GK, Boss ES, Picheral M, Guidi L, Pesant S, Scanlan DJ, Wincker
773 P, et al. 2018. Light color acclimation is a key process in the global ocean distribution of
774 *Synechococcus* cyanobacteria. *Proc Natl Acad Sci USA* 115:E2010–E2019.
- 775 Grébert T, Nguyen AA, Pokhrel S, Joseph KL, Ratin M, Dufour L, Chen B, Haney AM, Karty JA, Trinidad
776 JC, et al. 2021. Molecular bases of an alternative dual-enzyme system for light color acclimation of
777 marine *Synechococcus* cyanobacteria. *Proc Natl Acad Sci USA* 118:e2019715118.
- 778 Grindley NDF, Whiteson KL, Rice PA. 2006. Mechanisms of site-specific recombination. *Annu. Rev.*
779 *Biochem.* 75:567–605.
- 780 Guidi L, Chaffron S, Bittner L, Eveillard D, Larhlimi A, Roux S, Darzi Y, Audic S, Berline L, Brum J, et al.
781 2016. Plankton networks driving carbon export in the oligotrophic ocean. *Nature* 532:465–470.
- 782 Guindon S, Gascuel O. 2003. A simple, fast, and accurate algorithm to estimate large phylogenies by
783 maximum likelihood. *Syst. Biol.* 52:696–704.
- 784 Hackl T, Laurenceau R, Ankenbrand MJ, Bliem C, Cariani Z, Thomas E, Dooley KD, Arellano AA, Hogle
785 SL, Berube P, et al. 2020. Novel integrative elements and genomic plasticity in ocean ecosystems.
786 *BioRxiv*:2020.12.28.424599.
- 787 Haft DH, Basu MK, Mitchell DA. 2010. Expansion of ribosomally produced natural products: a nitrile
788 hydratase- and Nif11-related precursor family. *BMC Biol* 8:70.
- 789 Haverkamp T, Acinas SG, Doeleman M, Stomp M, Huisman J, Stal LJ. 2008. Diversity and phylogeny of
790 Baltic Sea picocyanobacteria inferred from their ITS and phycobiliprotein operons. *Environ*
791 *Microbiol* 10:174–188.
- 792 Herdman M, Castenholz RW, Waterbury JB, Rippka R. 2001. Form-genus XIII. *Synechococcus*. In: Boone
793 D, Castenholz R, editors. *Bergey's Manual of Systematics of Archaea and Bacteria Volume 1*. 2nd
794 Ed. New York: Springer-Verlag. p. 508–512.
- 795 Holtrop T, Huisman J, Stomp M, Biersteker L, Aerts J, Grébert T, Partensky F, Garczarek L, van der
796 Woerd HJ. 2021. Vibrational modes of water predict spectral niches for photosynthesis in lakes and
797 oceans. *Nature Ecol Evol* 5:55–66.

- 798 Huang S, Wilhelm SW, Harvey HR, Taylor K, Jiao N, Chen F. 2012. Novel lineages of *Prochlorococcus*
799 and *Synechococcus* in the global oceans. *ISME J* 6:285–297.
- 800 Huerta-Cepas J, Serra F, Bork P. 2016. ETE 3: Reconstruction, analysis, and visualization of
801 phylogenomic data. *Mol Biol Evol* 33:1635–1638.
- 802 Humily F, Farrant GK, Marie D, Partensky F, Mazard S, Perennou M, Labadie K, Aury J-M, Wincker P,
803 Segui AN, et al. 2014. Development of a targeted metagenomic approach to study in situ diversity
804 of a genomic region involved in light harvesting in marine *Synechococcus*. *FEMS Microbiol Ecol*
805 88:231–249.
- 806 Humily F, Partensky F, Six C, Farrant GK, Ratin M, Marie D, Garczarek L. 2013. A gene island with two
807 possible configurations is involved in chromatic acclimation in marine *Synechococcus*. *PLoS ONE*
808 8:e84459.
- 809 Kashtan N, Roggensack SE, Rodrigue S, Thompson JW, Biller SJ, Coe A, Ding H, Marttinen P, Malmstrom
810 RR, Stocker R, et al. 2014. Single-cell genomics reveals hundreds of coexisting subpopulations in
811 wild *Prochlorococcus*. *Science* 344:416–420.
- 812 Katoh K, Standley DM. 2013. MAFFT multiple sequence alignment software version 7: Improvements
813 in performance and usability. *Mol Biol Evol* 30:772–780.
- 814 Kronfel CM, Biswas A, Frick JP, Gutu A, Blensdorf T, Karty JA, Kehoe DM, Schluchter WM. 2019. The
815 roles of the chaperone-like protein CpeZ and the phycoerythrobilin lyase CpeY in phycoerythrin
816 biogenesis. *Biochim Biophys Acta Bioenerg* 1860:549–561.
- 817 Larsson J, Celepli N, Ininbergs K, Dupont CL, Yooseph S, Bergman B, Ekman M. 2014. Picocyanobacteria
818 containing a novel pigment gene cluster dominate the brackish water Baltic Sea. *ISME J* 8:1892–
819 1903.
- 820 Lassalle F, Périan S, Bataillon T, Nesme X, Duret L, Daubin V. 2015. GC-content evolution in bacterial
821 genomes: The biased gene conversion hypothesis expands. *PLOS Genetics* 11:e1004941.
- 822 Lee MD, Ahlgren NA, Kling JD, Walworth NG, Rocap G, Saito MA, Hutchins DA, Webb EA. 2019. Marine
823 *Synechococcus* isolates representing globally abundant genomic lineages demonstrate a unique
824 evolutionary path of genome reduction without a decrease in GC content. *Environ Microbiol*
825 21:1677–1686.
- 826 Magoč T, Salzberg SL. 2011. FLASH: Fast length adjustment of short reads to improve genome
827 assemblies. *Bioinformatics* 27:2957–2963.
- 828 Mahmoud RM, Sanfilippo JE, Nguyen AA, Strnat JA, Partensky F, Garczarek L, Abo El Kassem N, Kehoe
829 DM, Schluchter WM. 2017. Adaptation to blue light in marine *Synechococcus* requires MpeU, an
830 enzyme with similarity to phycoerythrobilin lyase isomerases. *Front Microbiol* 8:243.

- 831 Mazard S, Ostrowski M, Partensky F, Scanlan DJ. 2012. Multi-locus sequence analysis, taxonomic
832 resolution and biogeography of marine *Synechococcus*: Taxonomic resolution and biogeography of
833 marine *Synechococcus*. *Environ Microbiol* 14:372–386.
- 834 Mella-Flores D, Mazard S, Humily F, Partensky F, Mahé F, Bariat L, Courties C, Marie D, Ras J, Mauriac
835 R, et al. 2011. Is the distribution of *Prochlorococcus* and *Synechococcus* ecotypes in the
836 Mediterranean Sea affected by global warming? *Biogeosciences* 8:2785–2804.
- 837 Montgomery BL, Casey ES, Grossman AR, Kehoe DM. 2004. Apla, a member of a new class of
838 phycobiliproteins lacking a traditional role in photosynthetic light harvesting. *J Bacteriol* 186:7420–
839 7428.
- 840 Moore CM, Mills MM, Arrigo KR, Berman-Frank I, Bopp L, Boyd PW, Galbraith ED, Geider RJ, Guieu C,
841 Jaccard SL, et al. 2013. Processes and patterns of oceanic nutrient limitation. *Nature Geosci* 6:701–
842 710.
- 843 Moutin T, Van Wambeke F, Prieur L. 2012. Introduction to the Biogeochemistry from the Oligotrophic
844 to the Ultraoligotrophic Mediterranean (BOUM) experiment. *Biogeosciences* 9:3817–3825.
- 845 Olson RJ, Chisholm SW, Zettler ER, Armbrust EV. 1990. Pigment, size and distribution of *Synechococcus*
846 in the North Atlantic and Pacific oceans. *Limnol Oceanogr* 35:45–58.
- 847 Ong LJ, Glazer AN, Waterbury JB. 1984. An unusual phycoerythrin from a marine cyanobacterium.
848 *Science* 224:80–83.
- 849 Palenik B. 2001. Chromatic adaptation in marine *Synechococcus* strains. *Appl Environ Microbiol*
850 67:991–994.
- 851 Paulsen ML, Doré H, Garczarek L, Seuthe L, Müller O, Sandaa R-A, Bratbak G, Larsen A. 2016.
852 *Synechococcus* in the Atlantic gateway to the Arctic Ocean. *Front Mar Sci* 3:191.
- 853 Retchless AC, Lawrence JG. 2007. Temporal fragmentation of speciation in bacteria. *Science* 317:1093–
854 1096.
- 855 Retchless AC, Lawrence JG. 2010. Phylogenetic incongruence arising from fragmented speciation in
856 enteric bacteria. *Proc Natl Acad Sci USA* 107:11453–11458.
- 857 Sánchez-Baracaldo P, Bianchini G, Di Cesare A, Callieri C, Christmas NAM. 2019. Insights into the
858 evolution of picocyanobacteria and phycoerythrin genes (*mpeBA* and *cpeBA*). *Front Microbiol*
859 10:45.
- 860 Sanfilippo JE, Garczarek L, Partensky F, Kehoe DM. 2019. Chromatic acclimation in Cyanobacteria: A
861 diverse and widespread process for optimizing photosynthesis. *Annu Rev Microbiol* 73:407–433.
- 862 Sanfilippo JE, Nguyen AA, Garczarek L, Karty JA, Pokhrel S, Strnat JA, Partensky F, Schluchter WM,
863 Kehoe DM. 2019. Interplay between differentially expressed enzymes contributes to light color
864 acclimation in marine *Synechococcus*. *Proc Natl Acad Sci USA* 116:6457–6462.

- 865 Sanfilippo JE, Nguyen AA, Karty JA, Shukla A, Schluchter WM, Garczarek L, Partensky F, Kehoe DM.
866 2016. Self-regulating genomic island encoding tandem regulators confers chromatic acclimation to
867 marine *Synechococcus*. *Proc Natl Acad Sci USA* 113:6077–6082.
- 868 Scheer H, Zhao K-H. 2008. Biliprotein maturation: the chromophore attachment: Biliprotein
869 chromophore attachment. *Mol Microbiol* 68:263–276.
- 870 Schluchter WM, Shen G, Alvey RM, Biswas A, Saunée NA, Williams SR, Mille CA, Bryant DA. 2010.
871 Phycobiliprotein Biosynthesis in Cyanobacteria: Structure and Function of Enzymes Involved in
872 Post-translational Modification. In: Hallenbeck PC, editor. Recent Advances in Phototrophic
873 Prokaryotes. Vol. 675. Advances in Experimental Medicine and Biology. New York, NY: Springer New
874 York. p. 211–228. Available from: http://link.springer.com/10.1007/978-1-4419-1528-3_12
- 875 Shukla A, Biswas A, Blot N, Partensky F, Karty JAA, Hammad LAA, Garczarek L, Gutu A, Schluchter
876 WMM, Kehoe DMM. 2012. Phycoerythrin-specific bilin lyase-isomerase controls blue-green
877 chromatic acclimation in marine *Synechococcus*. *Proc Natl Acad Sci USA* 109:20136–20141.
- 878 Sidler WA. 1994. Phycobilisome and phycobiliprotein structure. In: Bryant DA, editor. The Molecular
879 Biology of Cyanobacteria. Advances in Photosynthesis. Dordrecht: Springer Netherlands. p. 139–
880 216. Available from: https://doi.org/10.1007/978-94-011-0227-8_7
- 881 Six C, Thomas J-C, Garczarek L, Ostrowski M, Dufresne A, Blot N, Scanlan DJ, Partensky F. 2007. Diversity
882 and evolution of phycobilisomes in marine *Synechococcus* spp.: a comparative genomics study.
883 *Genome Biol* 8:R259.
- 884 Six C, Thomas J-C, Thion L, Lemoine Y, Zal F, Partensky F. 2005. Two novel phycoerythrin-associated
885 linker proteins in the marine cyanobacterium *Synechococcus* sp. strain WH8102. *J Bacteriol*
886 187:1685–1694.
- 887 Sohm JA, Ahlgren NA, Thomson ZJ, Williams C, Moffett JW, Saito MA, Webb EA, Rocap G. 2016. Co-
888 occurring *Synechococcus* ecotypes occupy four major oceanic regimes defined by temperature,
889 macronutrients and iron. *ISME J* 10:333–345.
- 890 Swanson RV, Zhou J, Leary JA, Williams T, De Lorimier R, Bryant DA, Glazer AN. 1992. Characterization
891 of phycocyanin produced by *cpcE* and *cpcF* mutants and identification of an intergenic suppressor
892 of the defect in bilin attachment. *J Biol Chem* 267:16146–16154.
- 893 Szöllősi GJ, Rosikiewicz W, Boussau B, Tannier E, Daubin V. 2013. Efficient exploration of the space of
894 reconciled gene trees. *Syst Biol* 62:901–912.
- 895 Tajima F. 1983. Evolutionary relationship of DNA sequences in finite populations. *Genetics* 105:437–
896 460.
- 897 Tang W, van der Donk WA. 2012. Structural characterization of four prochlorosins: A novel class of
898 lantipeptides produced by planktonic marine cyanobacteria. *Biochemistry* 51:4271–4279.

- 899 Ulloa O, Henríquez-Castillo C, Ramírez-Flandes S, Plominsky AM, Murillo AA, Morgan-Lang C, Hallam
900 SJ, Stepanauskas R. 2021. The cyanobacterium *Prochlorococcus* has divergent light-harvesting
901 antennae and may have evolved in a low-oxygen ocean. *PNAS* 118:e2025638118.
- 902 Wilbanks SM, Glazer AN. 1993. Rod structure of a phycoerythrin II-containing phycobilisome. I.
903 Organization and sequence of the gene cluster encoding the major phycobiliprotein rod
904 components in the genome of marine *Synechococcus* sp. WH8020. *J Biol Chem* 268:1226–1235.
- 905 Wood A, Phinney D, Yentsch C. 1998. Water column transparency and the distribution of spectrally
906 distinct forms of phycoerythrin-containing organisms. *Mar Ecol Prog Ser* 162:25–31.
- 907 Wu D, Jospin G, Eisen JA. 2013. Systematic identification of gene families for use as “markers” for
908 phylogenetic and phylogeny-driven ecological studies of Bacteria and Archaea and their major
909 subgroups. *PLOS ONE* 8:e77033.
- 910 Xia X, Guo W, Tan S, Liu H. 2017. *Synechococcus* assemblages across the salinity gradient in a salt wedge
911 estuary. *Front Microbiol* 8:1254.
- 912 Xia X, Liu H, Choi D, Noh JH. 2018. Variation of *Synechococcus* pigment genetic diversity along two
913 turbidity gradients in the China Seas. *Microb Ecol* 75:10–21.
- 914 Xia X, Partensky F, Garczarek L, Suzuki K, Guo C, Yan Cheung S, Liu H. 2017. Phylogeography and
915 pigment type diversity of *Synechococcus* cyanobacteria in surface waters of the northwestern
916 pacific ocean. *Environ Microbiol* 19:142–158.
- 917 Yu MH, Glazer AN. 1982. Cyanobacterial phycobilisomes. Role of the linker polypeptides in the
918 assembly of phycocyanin. *J Biol Chem* 257:3429–3433.
- 919 Zhou J, Gasparich GE, Stirewalt VL, De Lorimier R, Bryant DA. 1992. The *cpcE* and *cpcF* genes of
920 *Synechococcus* sp. PCC 7002: Construction and phenotypic characterization of interposon mutants.
921 *J Biol Chem* 267:16138–16145.
- 922 Zwirgmaier K, Jardillier L, Ostrowski M, Mazard S, Garczarek L, Vaultot D, Not F, Massana R, Ulloa O,
923 Scanlan DJ. 2008. Global phylogeography of marine *Synechococcus* and *Prochlorococcus* reveals a
924 distinct partitioning of lineages among oceanic biomes. *Environ Microbiol* 10:147–161.
- 925
- 926

927

Tables

928 **Table 1: Frequency of transfer events inferred by ALE for genes**
 929 **of the PBS rod region**

Gene category	Evolutionary event	Min.	Median	Mean	Max.
PBS	Duplications	0.00	0.00	1.019	19.09
PBS	Transfers	8.72	24.05	23.52	34.57
PBS	Losses	20.10	37.92	38.50	68.31
PBS	Speciations	64.70	94.36	93.08	138.01
Other	Duplications	0.00	0.00	0.56	71.11
Other	Transfers	0.00	12.91	14.80	100.68
Other	Losses	5.22	25.38	27.53	222.40
Other	Speciations	28.01	94.19	91.32	369.02

930

931

932 **Table 2: Frequency of transfer events inferred by ALE for genes**
 933 **of the PBS rod region**

934

Gene category	Transfer event	Min.	Median	Mean	Max.
PBS	Intra-clade	5.26	9.66	9.66	13.41
PBS	Extra-clade	2.08	14.57	13.86	21.29
PBS	Intra-PT	3.91	11.69	11.41	19.77
PBS	Extra-PT	4.51	12.74	12.11	17.42
Other	Intra-clade	0.00	8.31	8.42	40.07
Other	Extra-clade	0.00	4.33	6.14	81.73
Other	Intra-PT	0.00	5.97	6.29	40.57
Other	Extra-PT	0.00	6.94	8.27	68.06

935

936

937

Legends to Figures

938

939 **Fig. 1: PBS rod region for strains of different pigment types.** Regions are oriented from
 940 the phenylalanine tRNA (left) to the conserved low molecular weight tyrosine phosphatase
 941 *ptpA* (right). Genes are coloured according to their inferred function (as indicated in insert).
 942 Their length is proportional to the gene size and their thickness to the protein identity between
 943 strains of the same pigment type. The strains represented here are WH5701 (PT 1), WH7805
 944 (PT 2A), RS9907 (PT 3a), KORDI-100 (PT 3f), RS9916 (PT 3dA), WH8102 (PT 3c) and A15-
 945 62 (PT 3dB). Abbreviations: PC, phycocyanin; PE-I, phycoerythrin-I; PE-II, phycoerythrin-II;
 946 PBS, phycobilisomes.

947

948 **Fig. 2: Examples of tycheposons at 5' end of PBS regions.** Regions are oriented from the
 949 phenylalanine tRNA (tRNA-Phe) to *unk1*, the first coding gene of the PBS region. Genes
 950 putatively involved in DNA rearrangements (recombination, transposition, etc.) are colored and
 951 their orthologs in different regions are shown with the same color. Coding sequences with no
 952 gene name are either hypothetical, conserved hypothetical or pseudogenes. Gene length is
 953 proportional to the gene size. Abbreviations: TR, tyrosine recombinase; TPR, tetratricopeptide.
 954 The number after a gene name corresponds to its CLOG number in the Cyanorak database
 955 (Garczarek et al. 2021).

956

957 **Fig. 3: Characterization of PBS rod regions from natural population of *Synechococcus*.**
 958 (A) location of sampling sites used for fosmid library construction. (B) *Synechococcus* genetic
 959 diversity at each station, as assessed with the phylogenetic marker *petB*. (C) *mpeBA*
 960 phylogeny for isolates (black) and fosmids (gray). Squares and circles on right hand side
 961 correspond to reference strains and fosmids, respectively. Within PT 3dA, symbols with a blue

962 center and a red contour correspond to PT 3aA (the reference 3aA strain, MVIR-18-1, exhibits
 963 a constitutive low $Exc_{C495:545}$), and those with a blue center and a yellow contour to PT 3cA (the
 964 reference 3cA strain, BIOS-E4-1, exhibits a constitutive high $Exc_{C495:545}$; see text as well as
 965 Humily et al. 2013 and Grébert et al. 2018). Bootstrap values higher or equal to 90% are
 966 indicated by black circles, those comprised between 70% and <90% by empty circles, while
 967 no circles indicate values lower than 70%.

968

969 **Fig. 4: partial or complete PBS rod region retrieved from natural populations.** (A)
 970 Description of a new genomic organization related to 3dA pigment type with the CA4-A
 971 genomic island inserted at the 5'-end of the PBS rod genomic region. The PBS rod and CA4-
 972 A genomic regions of strain BL107 (3dA/clade IV) is shown as a reference. (B) Contigs other
 973 than those in (A) and longer than 10 kb, sorted according to their organization and inferred
 974 corresponding pigment type. Colors represent the clade of the strain giving the best BlastX hit
 975 within the given pigment type. The highly conserved *mpeBA* operon is shaded in gray.

976

977 **Fig. 5: Correspondence between phylogenies for the *mpeBA* operon and the marker**
 978 **gene *petB*, which reproduces the core genome phylogeny.** The pigment type for each
 979 strain is indicated by a coloured square in the *mpeBA* phylogeny, and its clade similarly
 980 indicated in the *petB* phylogeny. Bootstrap values higher or equal to 90% are indicated by
 981 black circles, those comprised between 70% and <90% by empty circles, while no circles
 982 indicate values lower than 70%.

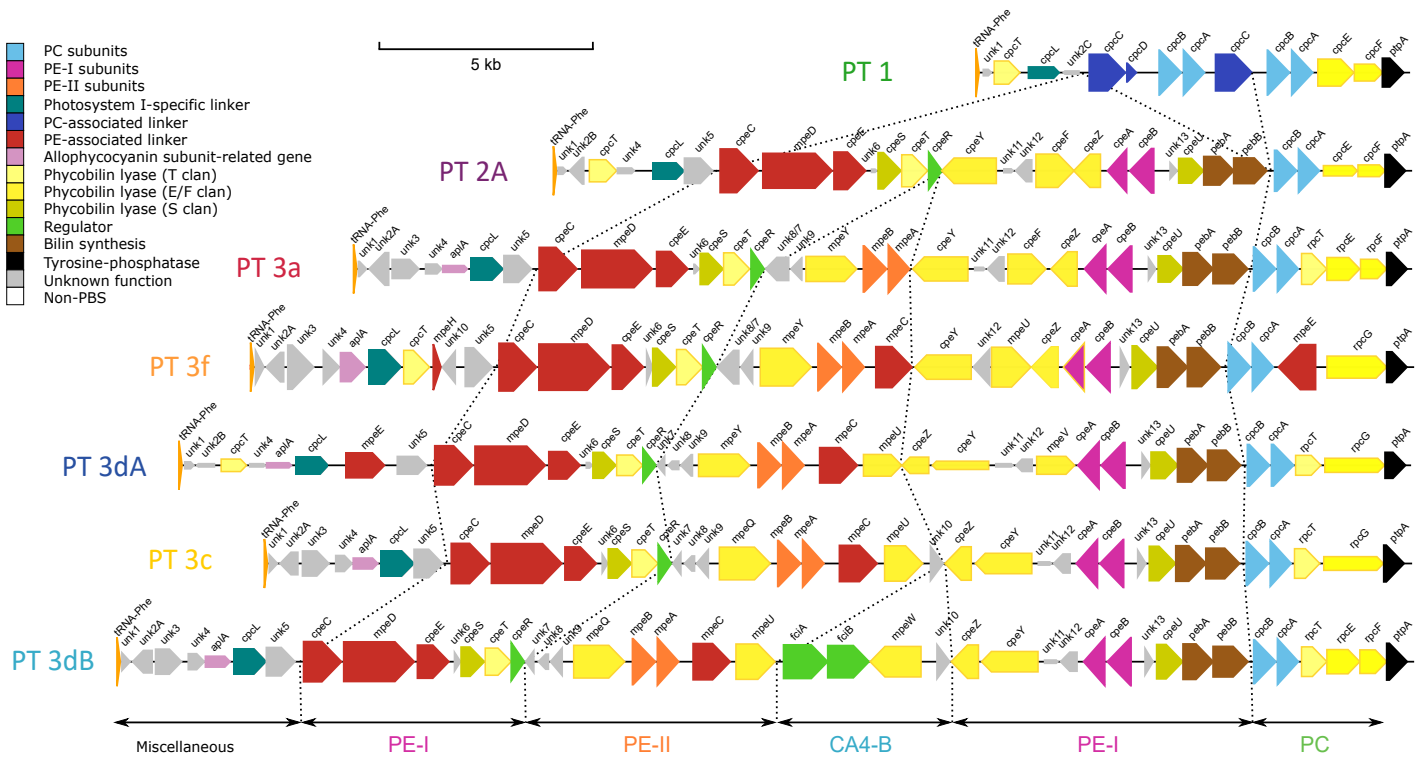
983

984 **Fig. 6: Evolutionary events affecting genes present in more than half of the analysed**
 985 **genomes inferred by reconciling gene trees with the species tree.** Genes were classified

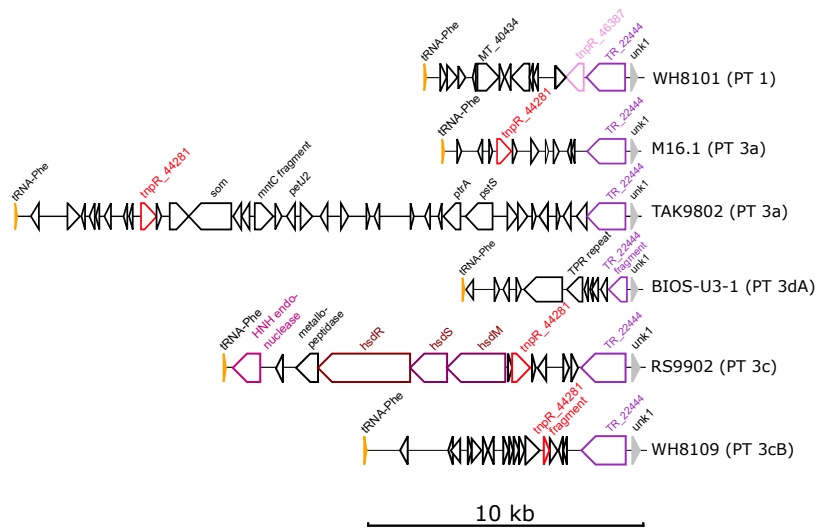
986 either as belonging to the PBS rod region (“PBS genes”) or as other genes (“Other”). *P*-values
987 for Wilcoxon rank sum exact test are shown.

988

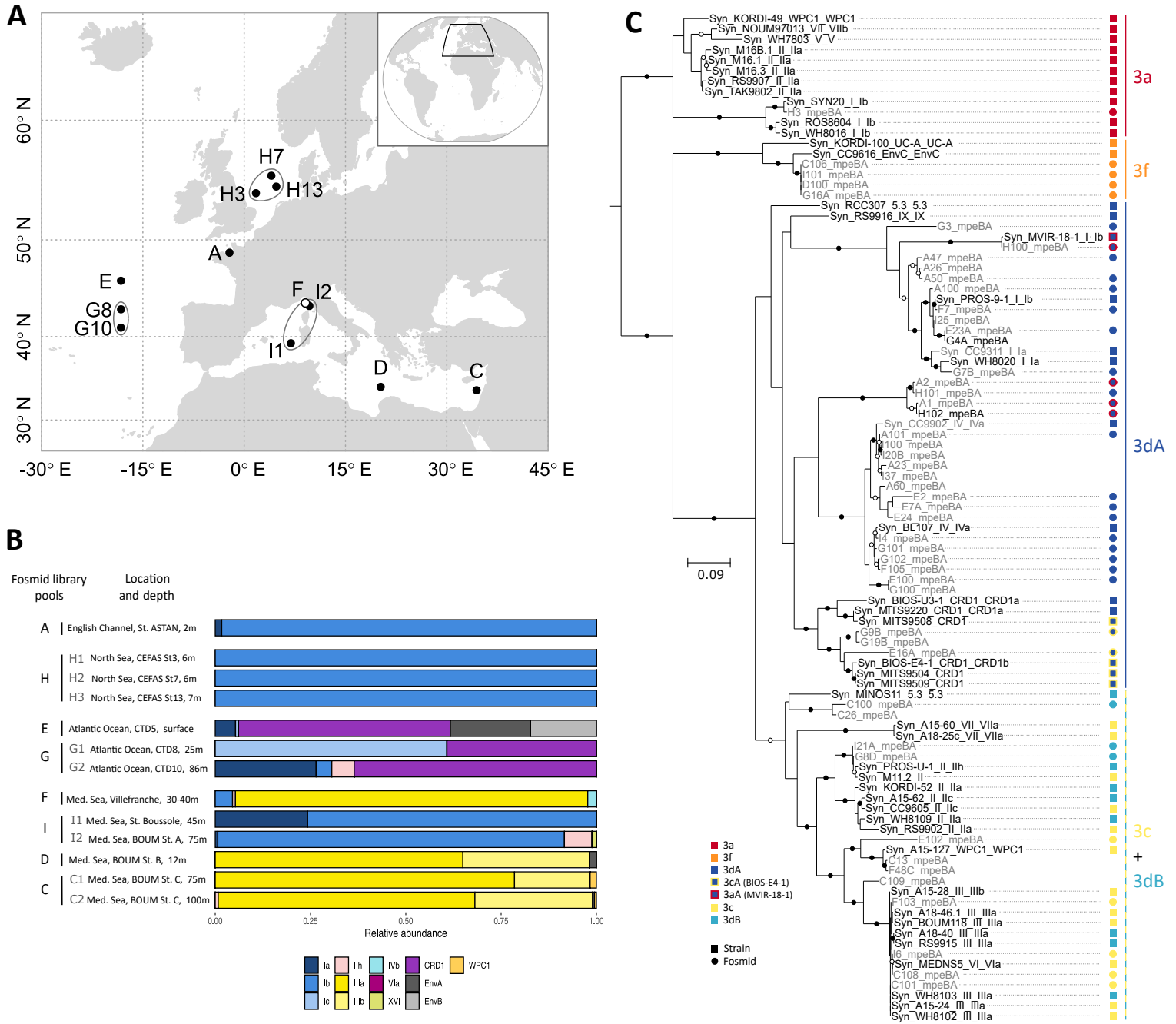
989 **Fig. 7: Putative evolutionary scenario for the occurrence of the different *Synechococcus***
990 **PT 3 subtypes.** This scenario is congruent with individual phylogenies of genes in the PBS
991 rod region. Note that the 5'- and 3'- end of the PBS rod region are cropped for better
992 visualisation of the PE-I/PE-II sub-regions. Genes that changed between two consecutive PT
993 precursor steps are highlighted by black contours (instead of blue for the other genes).



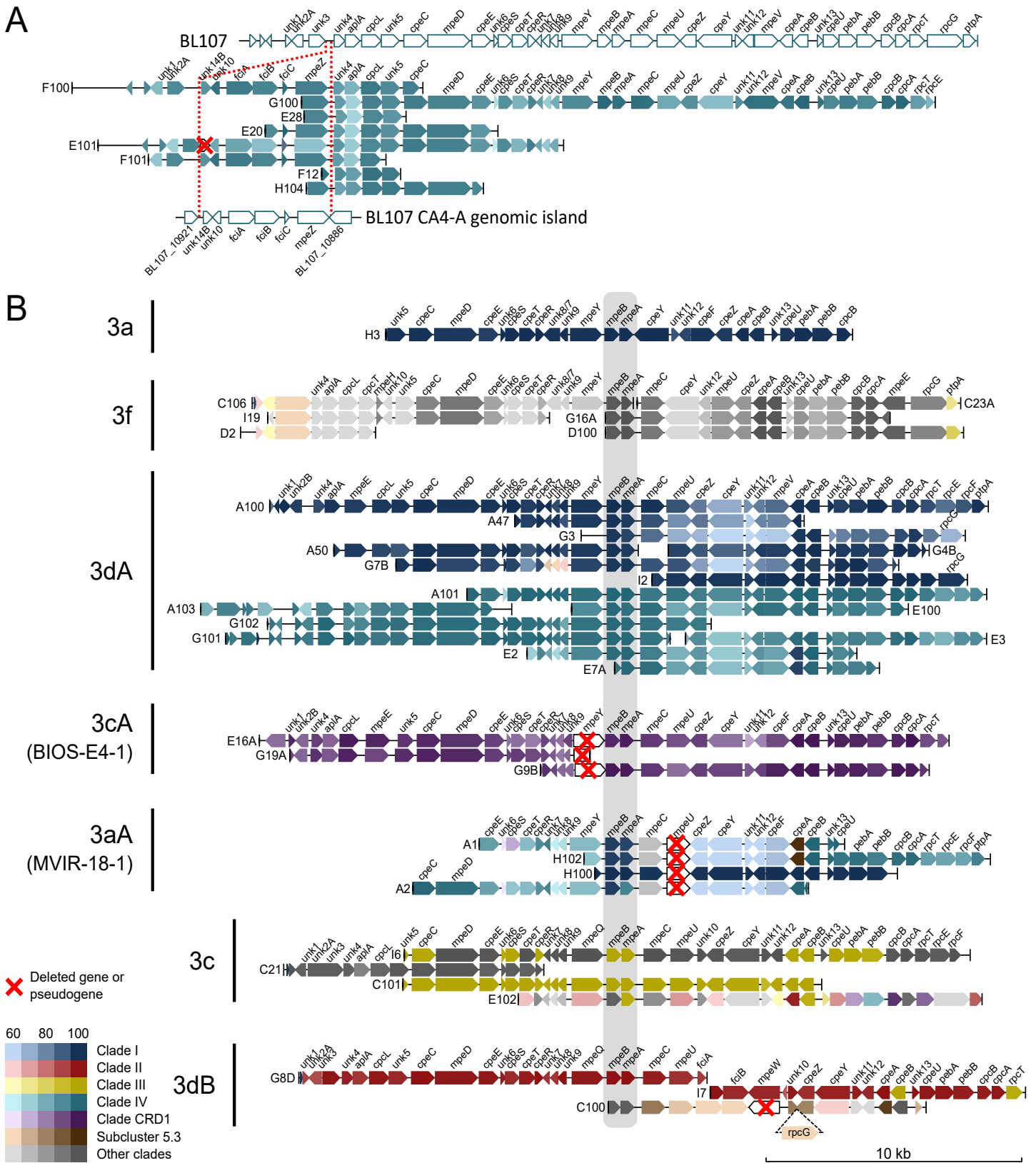
Grébert et al. Fig. 1



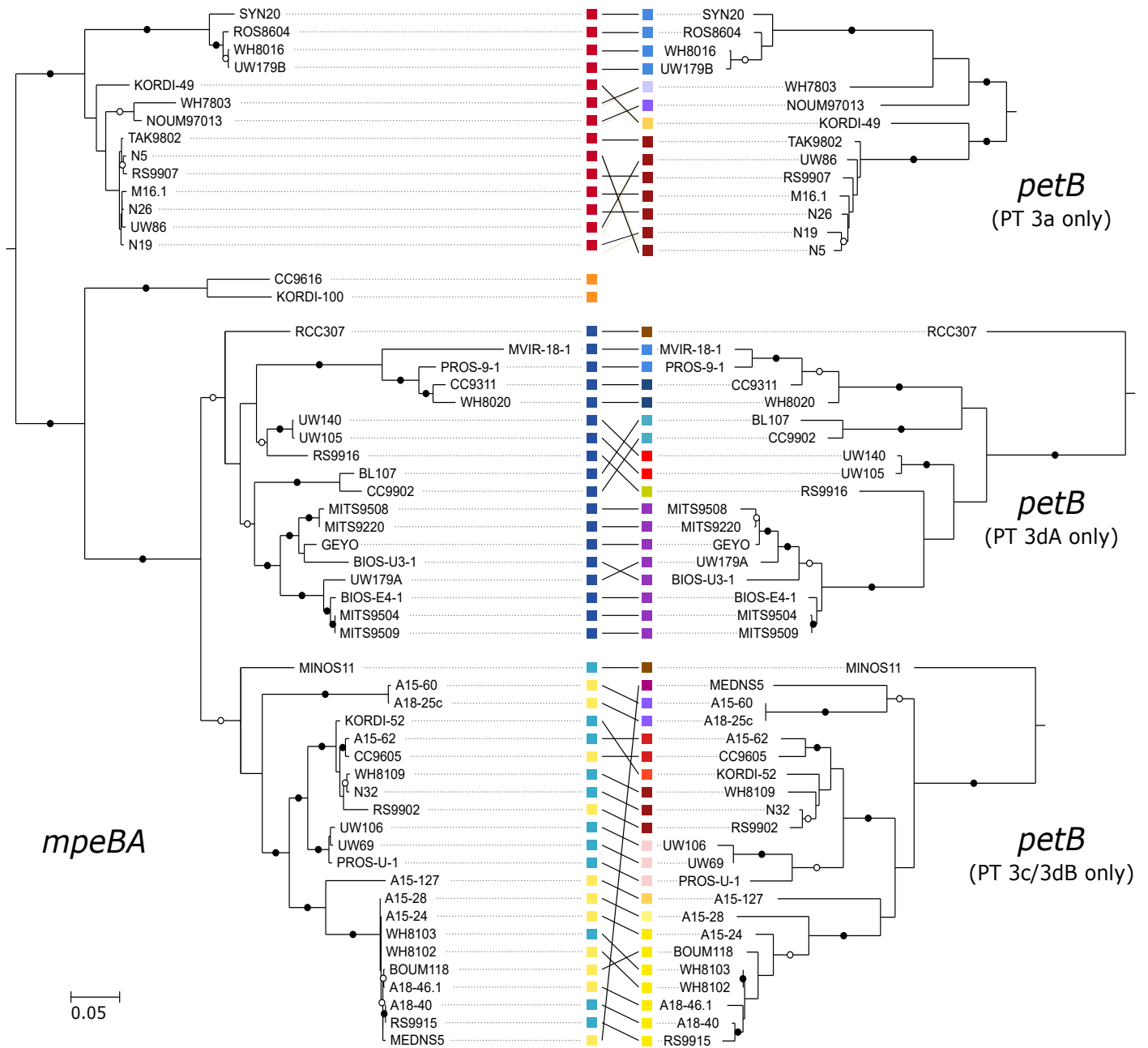
Grébert et al. Fig. 2



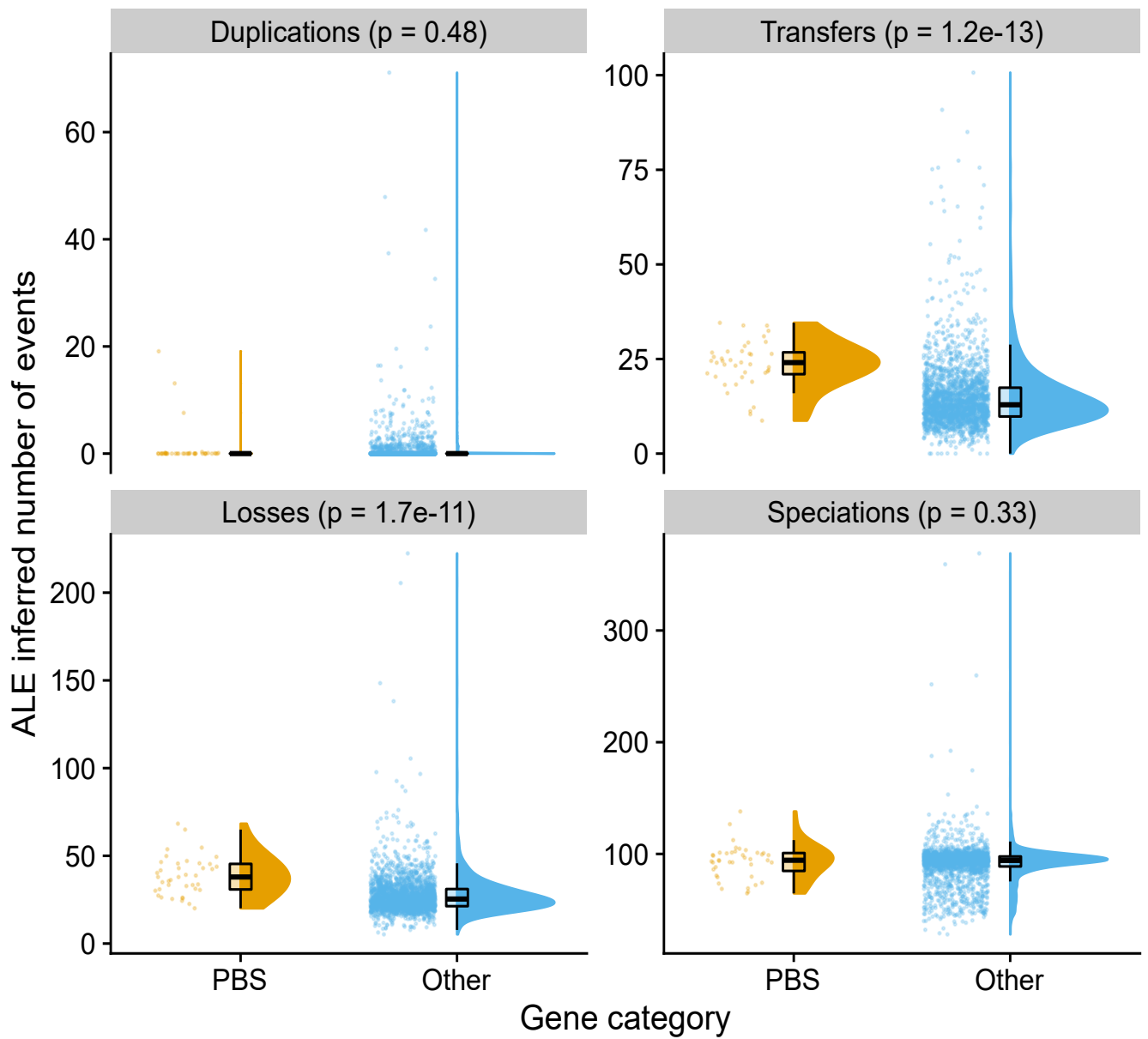
Grébert et al. Fig. 3



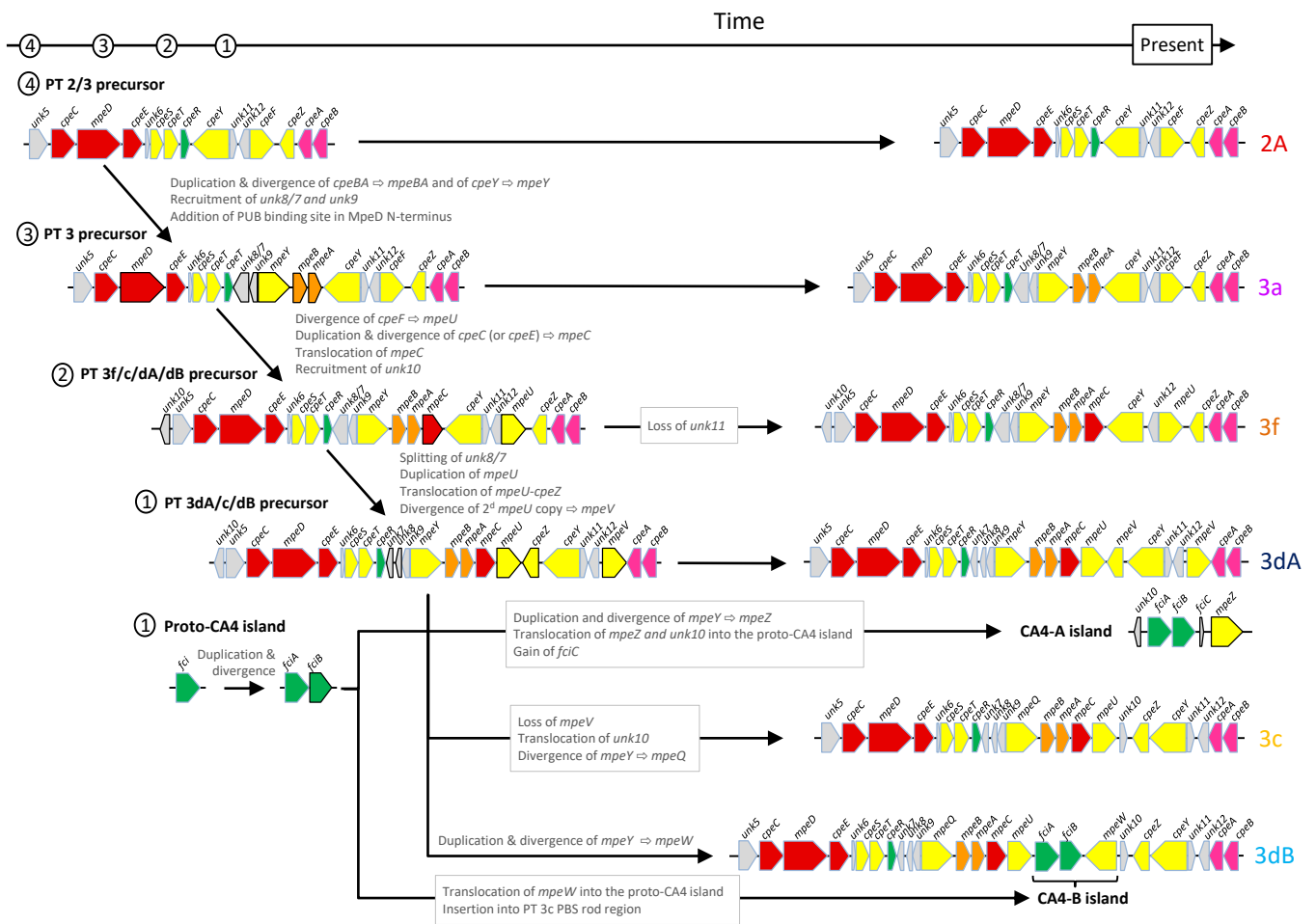
Grébert et al. Fig. 4



Grébert et al. Fig. 5



Grébert et al. Fig. 6



Grébert et al. Fig. 7

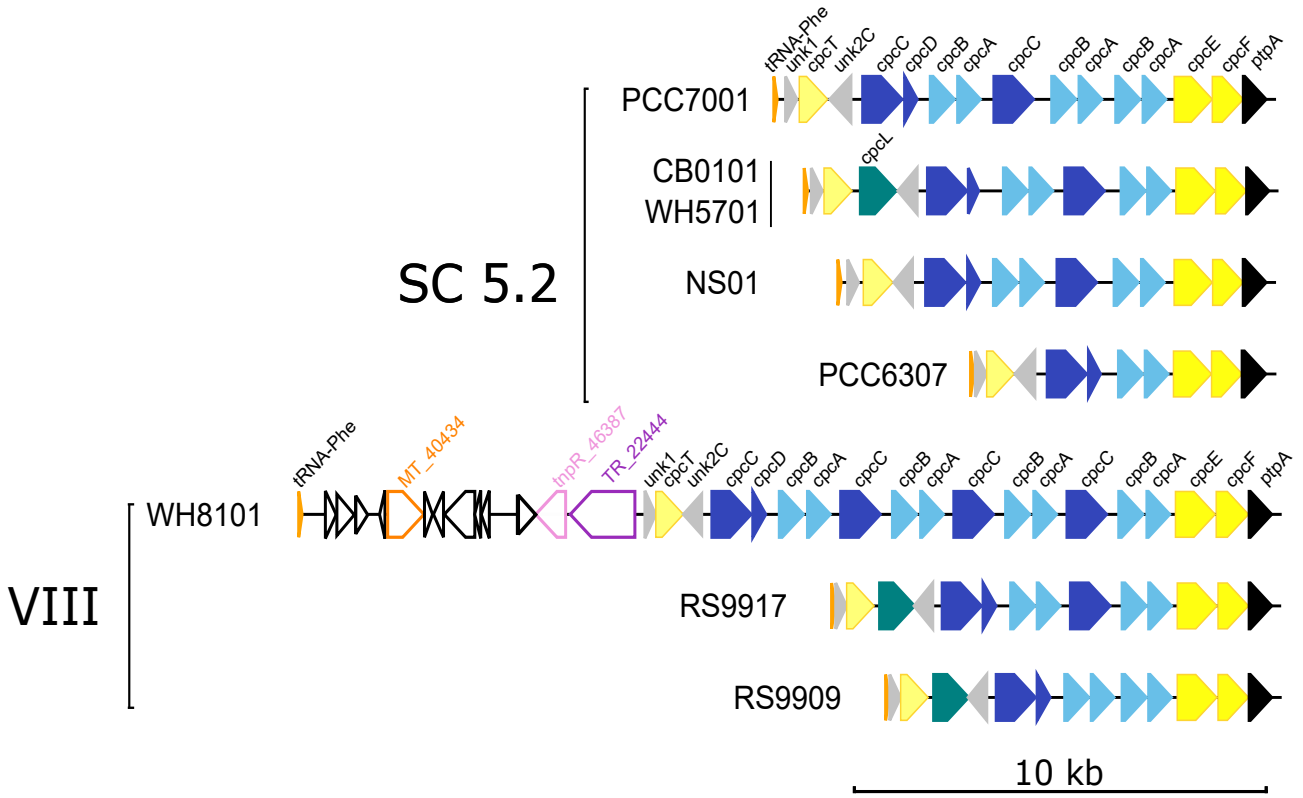


Fig. S1: PBS rod region for all pigment type 1 strains.

Regions are oriented from the phenylalanine tRNA to the conserved tyrosine phosphatase gene *ptpA*. PBS genes are colored according to their inferred function (see insert in Fig. 1) and their length is proportional to the gene size. Abbreviations: TR, tyrosine phosphatase, MT, methyltransferase. Genes with a black contour code for hypothetical or conserved hypothetical proteins. The number after some gene names corresponds to the CLOG number in the Cyanorak information system, e.g. CK_00040434 (Garczarek et al. 2021).

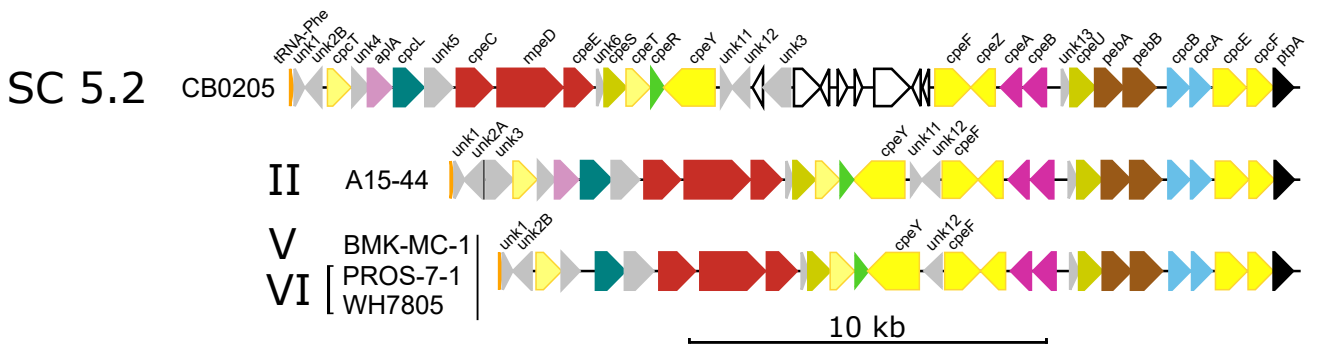


Fig. S2: Same as Fig. S1 but for pigment type 2.

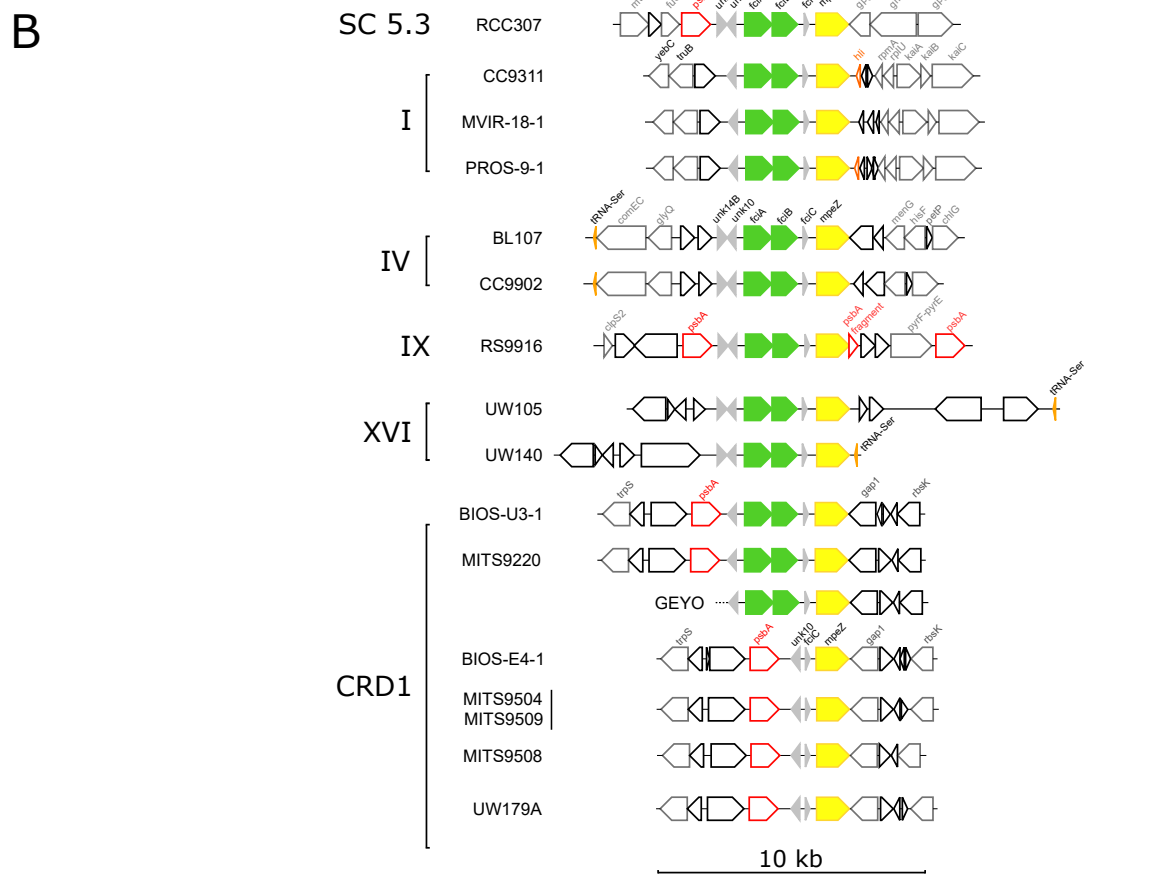
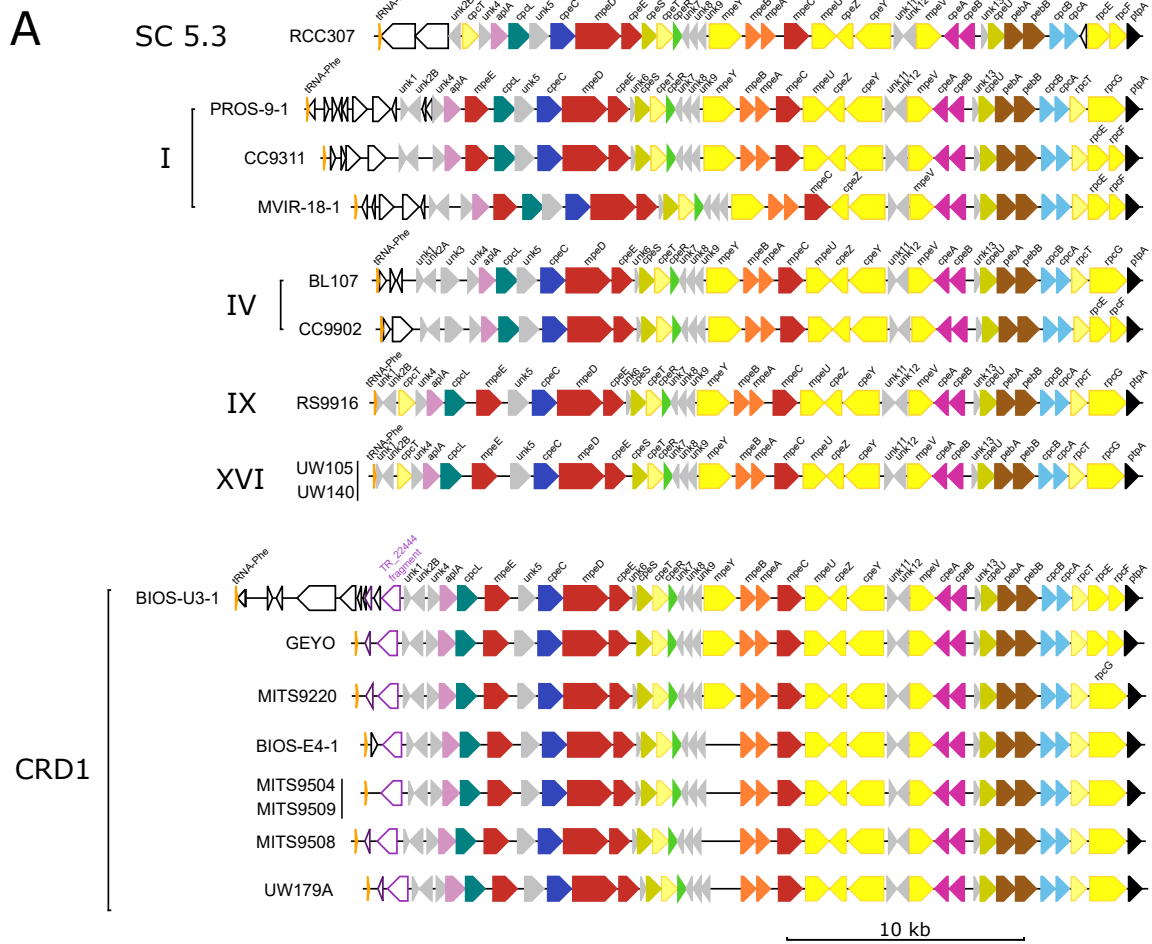


Fig. S5: PBS rod region and CA4-A island for all strains of pigment type 3dA.
 (A) PBS rod region. (B) CA4-A genomic island and surrounding genes. Solid arrows represent genes from the CA4-A genomic island and are colored according to their inferred function (see insert in Fig. 1). Genes with a black contour code for hypothetical or conserved hypothetical proteins and those with a grey contour to genes of known function not linked to PBS. Recombination hotspots such as tRNAs, *psbA* or *hli* genes are also shown in color. PBS regions that have identical configurations in several strains are shown only once.

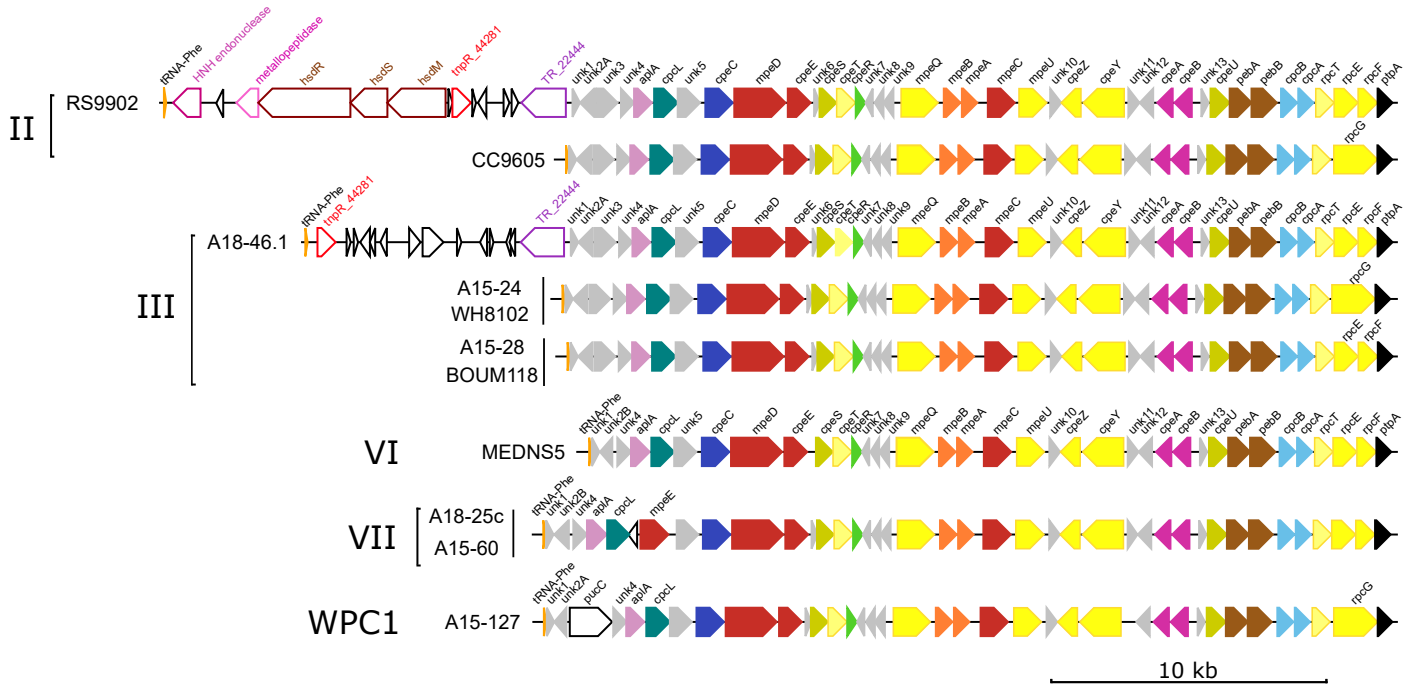


Fig. S6: Same as Fig. S1 but for pigment type 3c.

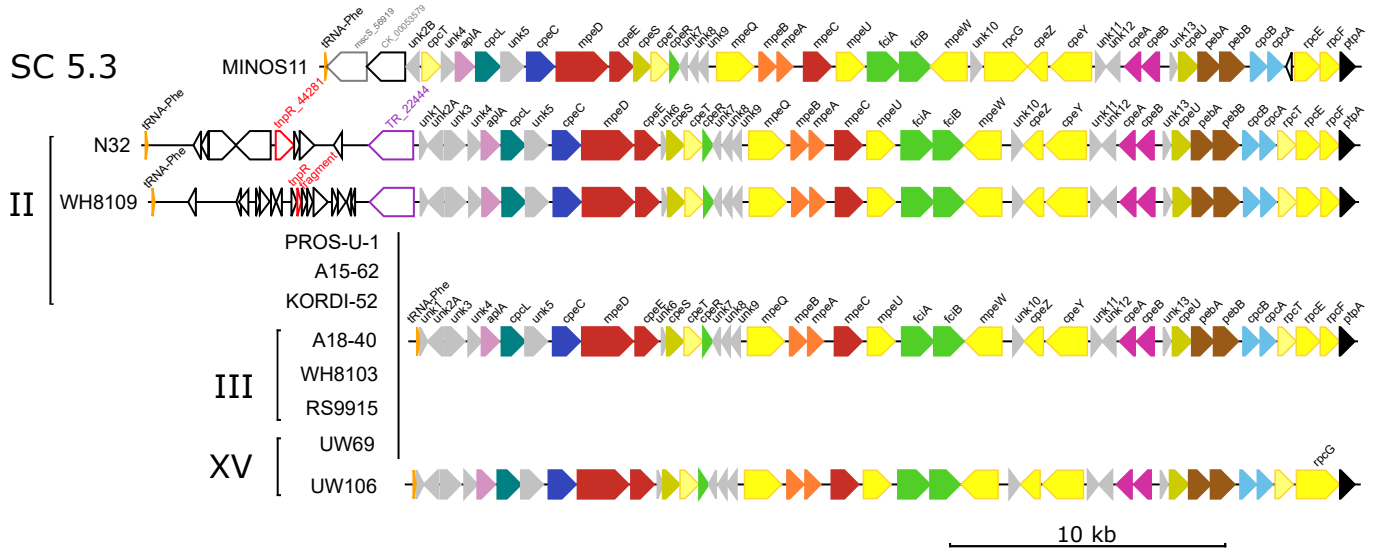


Fig. S7: Same as Fig. S1 but for pigment type 3dB.

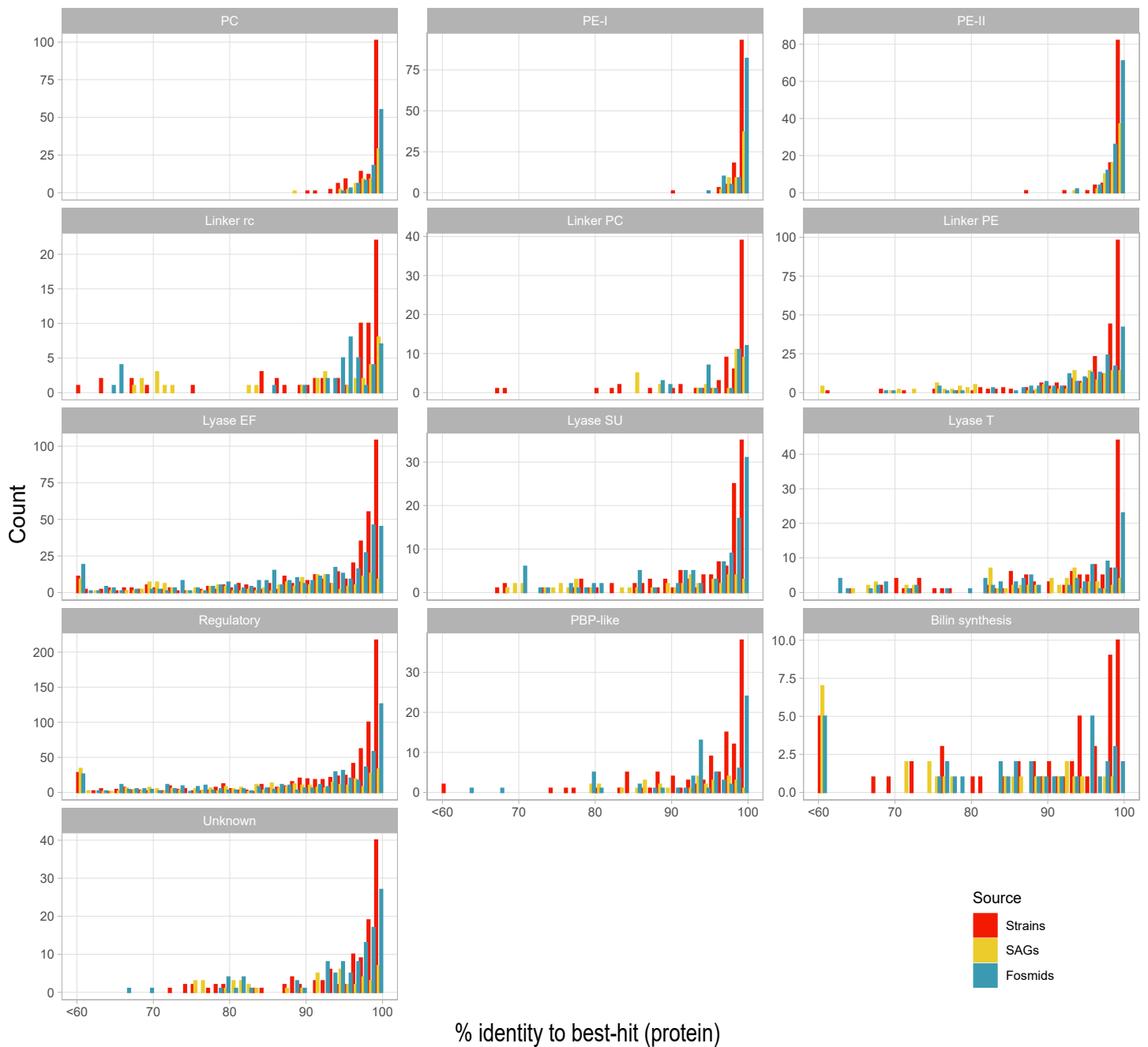
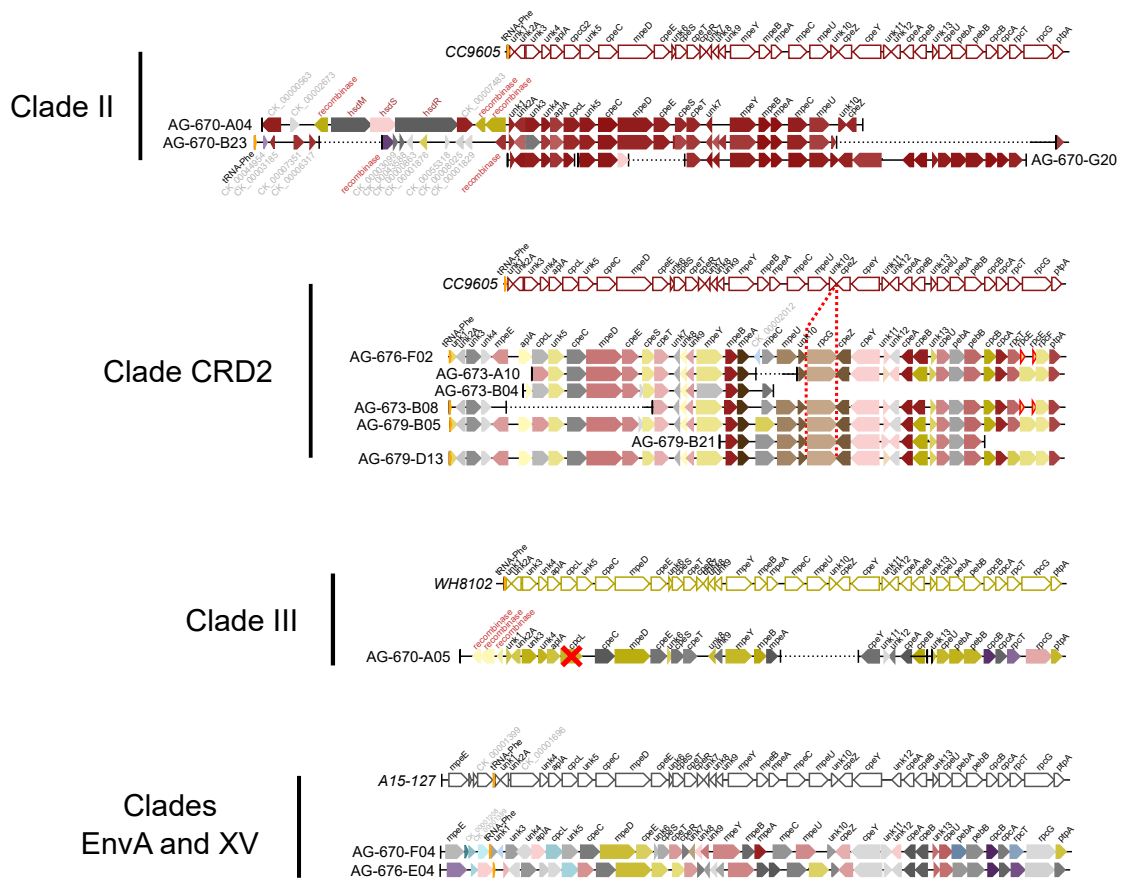
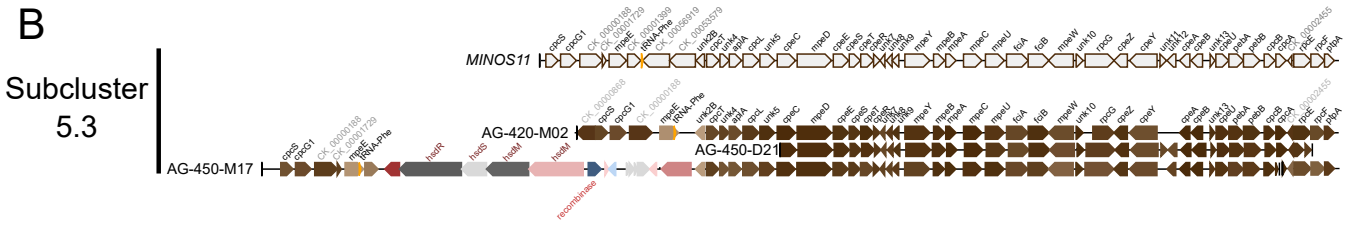


Fig. S8: Genetic variability of the different proteins encoded in the PBS rod genomic region, grouped by functional categories. For each group of orthologous proteins, identity is based on the blastp best-hit other than self-hit for strains, and blastp best-hit to all strains for fosmids and SAGs, and results for each group of orthologs have then be gathered by functional categories as follows: PC, phycocyanin (CpcA/B, RpcA/B); PE-I, phycoerythrin-I (CpeA/B); PE-II, phycoerythrin-II (MpeA/B); Linker rc, linker rod-core-like (CpcL); Linker PC, PC-associated linker (CpcC, CpcD, CpeC); Linker PE, PE-associated linker (CpeE, MpeC, MpeD, MpeE, MpeH); lyase EF, lyase of the E/F clan (CpeF, CpeY, CpeZ, MpeU, MpeY, MpeW, MpeZ, RpcE, RpcF, RpcG, CpcE, CpcF); lyase SU, lyase of the S/U clan (CpeS, CpeU); lyase T, lyase of the T clan (CpcT, CpeT, RpcT); Unknown, uncharacterized conserved hypothetical proteins (Unk1 through 13, Unk2A, Unk2B, Unk2C, Unk8/7, Unk14B).

A



B



C

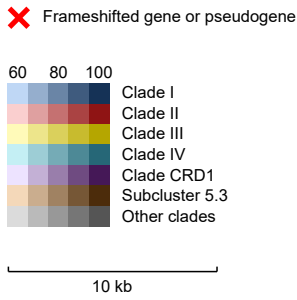
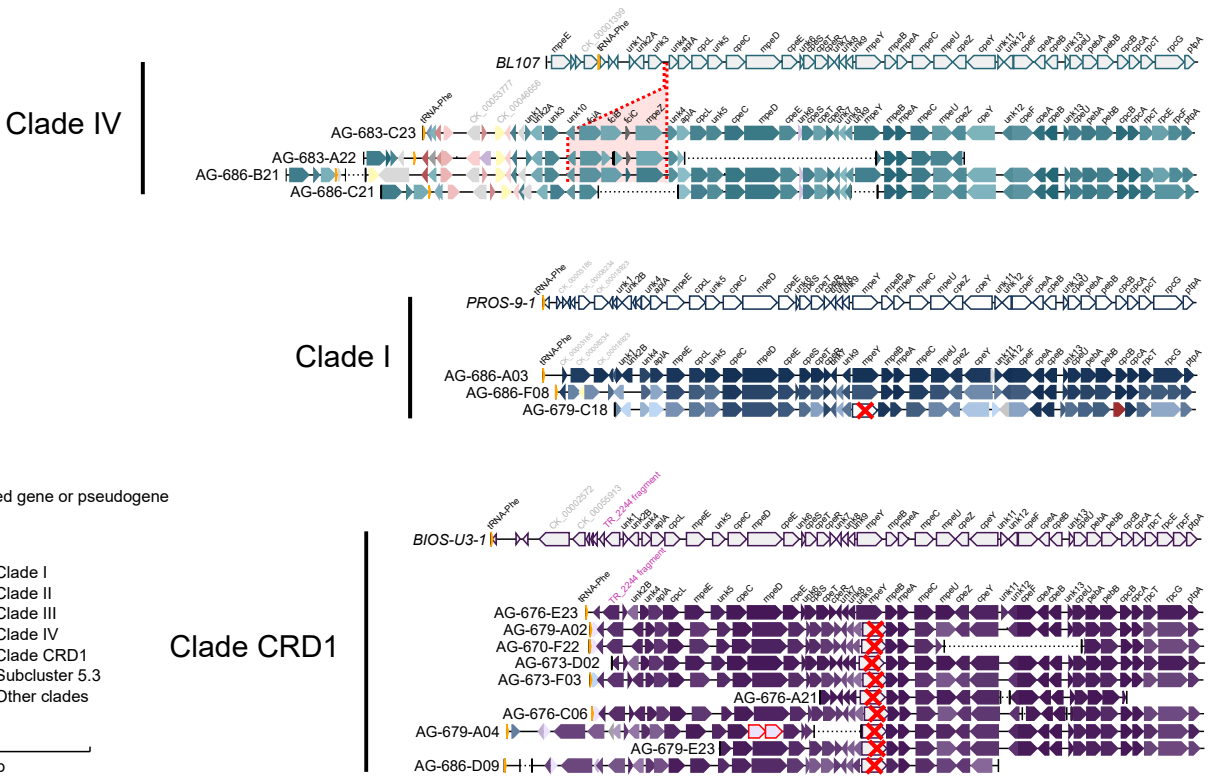


Fig. S9: partial or complete PBS rod region retrieved from single-cell amplified genomes (SAGs). PBS regions are grouped by pigment type, with PT 3c in (A), PT 3dB in (B) and PT 3dA in (C). Colors represent the clade of the reference strain giving the best blastp hit within the given pigment type.

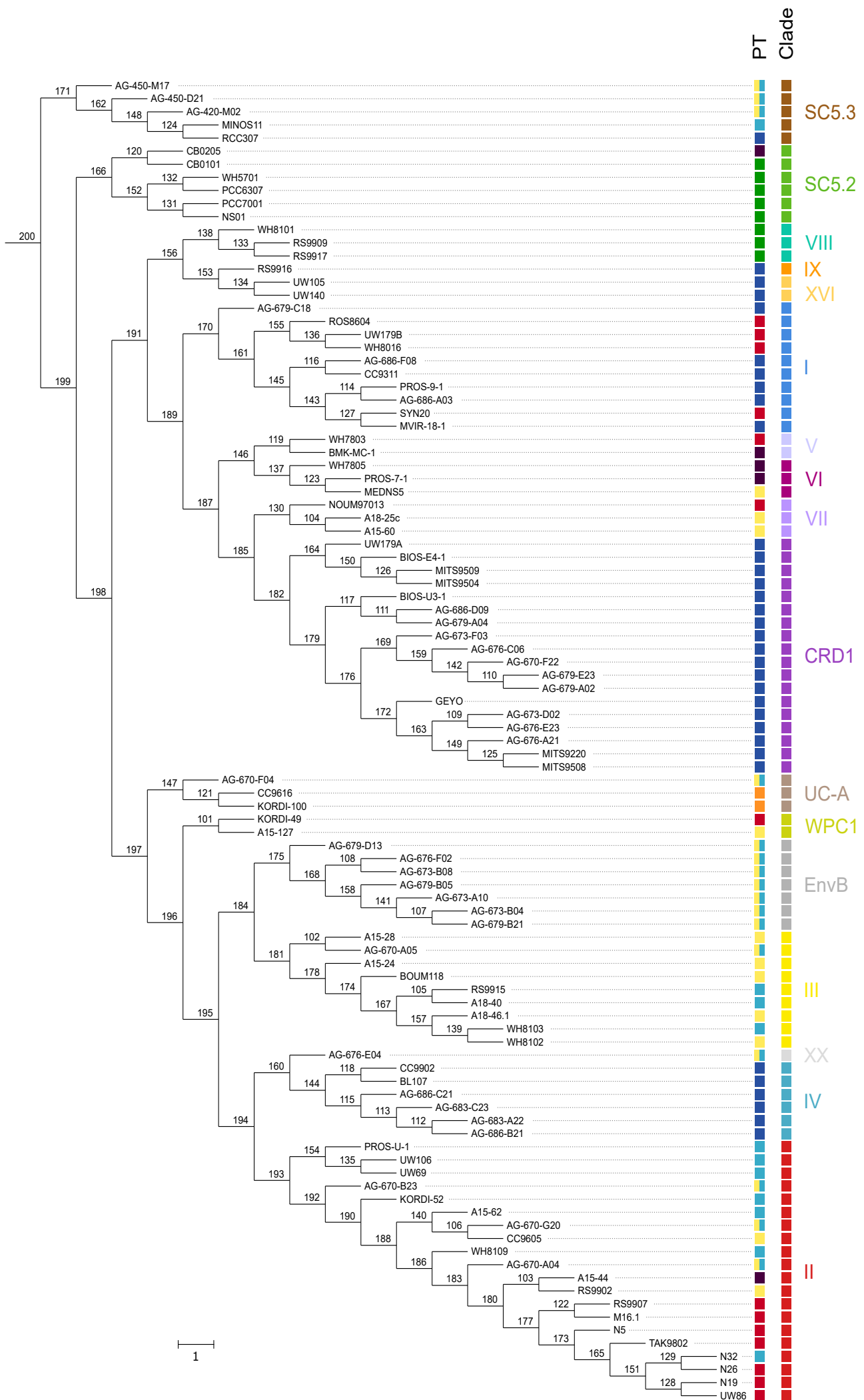


Fig. S10: Reference species tree based on 73 core proteins used in ALE analysis. All internal nodes are labelled according to ALE numbering, allowing identification of transfer events from/to internal nodes.

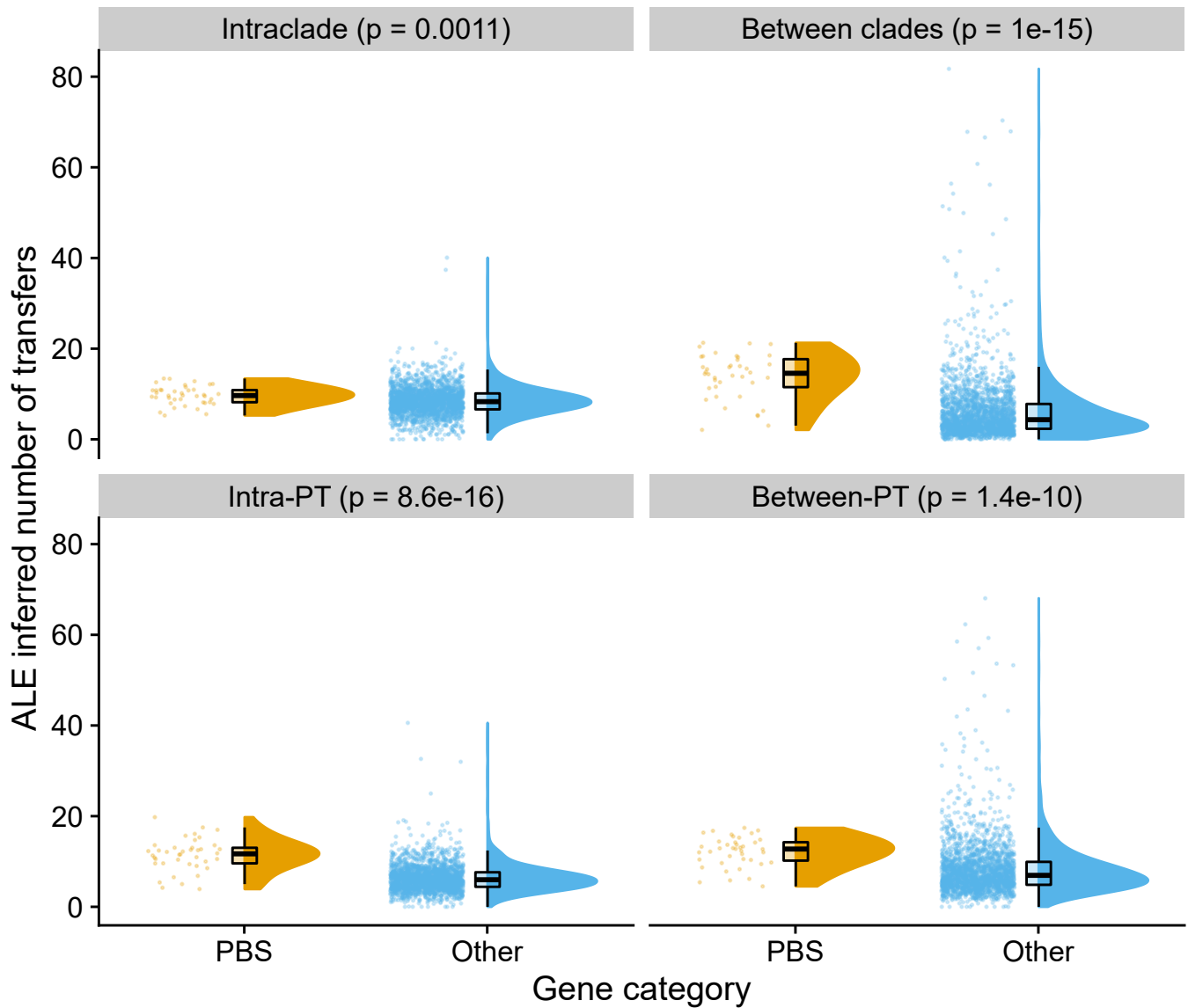


Fig. S11: Comparison of the distribution of transfer events inferred by ALE for gene belonging to the PBS rod region (PBS) and other genes (Other).

Transfer events were classified as intraclade if they involved two strains or ancestral lineages from the same clade, and between clades otherwise. Similarly, transfers were classified as intra-pigment type (Intra-PT) if they involved two strains or ancestral lineages having the same pigment type, and between pigment types (Between-PT) otherwise. P-values for Wilcoxon rank sum exact test are reported.